Thesis for the Degree of Doctor of Philosophy

Sparse Array Architectures for Wireless Communication and Radar Applications

Navid Amani

CHALMERS

Department of Electrical Engineering
Antenna Systems Group
Chalmers University of Technology

Göteborg, Sweden 2021

Sparse Array Architectures for Wireless Communication and Radar Applications

Navid Amani

ISBN 978-91-7905-572-1

Doktorsavhandlingar vid Chalmers tekniska högskola
Ny serie nr 5039
ISSN 0346-718X

Department of Electrical Engineering
Antenna Systems Group
Chalmers University of Technology
SE–412 96 Göteborg
Sweden
Telephone: +46 (0)31 – 772 1000
Email: anavid@chalmers.se

Typeset by the author using LaTeX.

Chalmers Reproservice
Göteborg, Sweden 2021

Sparse Array Architectures for Wireless Communication and Radar Applications

PROEFSCHRIFT

ter verkrijging van de graad van doctor aan de Technische Universiteit Eindhoven, op gezag van de rector magnificus prof.dr.ir. F.P.T. Baaijens, voor een commissie aangewezen door het College voor Promoties, in het openbaar te verdedigen op vrijdag 5 november 2021 om 16:00 uur

door

Navid Amani

geboren te Amol, Iran

Dit proefschrift is goedgekeurd door de promotoren en de samenstelling van de promotiecommissie is als volgt:

1e promotor:	dr.ir. R. Maaskant	(Chalmers University of Technology)
2e promotor:	prof.dr.ir. A. B. Smolders	
co-promotor(en):	prof.dr.ir. M. V. Ivashina	(Chalmers University of Technology)
	dr.ir. U. Johannsen	
leden:	prof.dr.ir. M. A. Jensen	(Brigham Young University)
	prof.dr.ir. S. M. Heemstra de Groot	
	prof.dr.ir. B. Göransson	(KTH Royal Institute of Technology)
	prof.dr.ir. T. Rylander	(Chalmers University of Technology)
adviseur(s):	ir. W. Van Cappellen	(Netherlands Institute for Radio Astronomy)
	dr.ir. A. Filippi	(NXP Semiconductors)

Het onderzoek of ontwerp dat in dit proefschrift wordt beschreven is uitgevoerd in overeenstemming met de TU/e Gedragscode Wetenschapsbeoefening.

To my family

Abstract

This thesis focuses on sparse array architectures for the next generation of wireless communication, known as fifth-generation (5G), and automotive radar direction-of-arrival (DOA) estimation. For both applications, array spatial resolution plays a critical role to better distinguish multiple users/sources. Two novel base station antenna (BSA) configurations and a new sparse MIMO radar, which both outperform their conventional counterparts, are proposed.

We first develop a multi-user (MU) multiple-input multiple-output (MIMO) simulation platform which incorporates both antenna and channel effects based on standard network theory. The combined transmitter-channel-receiver is modeled by cascading **Z**-matrices to interrelate the port voltages/currents to one another in the linear network model. The herein formulated channel matrix includes physical antenna and channel effects and thus enables us to compute the actual port powers. This is in contrast with the assumptions of isotropic radiators without mutual coupling effects which are commonly being used in the "*Wireless Community*".

Since it is observed in our model that the sum-rate of a MU-MIMO system can be adversely affected by antenna gain pattern variations, a novel BSA configuration is proposed by combining field-of-view (FOV) sectorization, array panelization and array sparsification. A multi-panel BSA, equipped with sparse arrays in each panel, is presented with the aim of reducing the implementation complexities and maintaining or even improving the sum-rate.

We also propose a capacity-driven array synthesis in the presence of mutual coupling for a MU-MIMO system. We show that the appearance of grating lobes is degrading the system capacity and cannot be disregarded in a MU communication, where space division multiple access (SDMA) is applied. With the aid of sparsity and aperiodicity, the adverse effects of grating lobes and mutual coupling are suppressed and capacity is enhanced. This is performed by proposing a two-phase optimization. In Phase I, the problem is relaxed to a convex optimization by ignoring the mutual coupling and weakening the constraints. The solution of Phase I is used as the initial guess for the genetic algorithm (GA) in phase II, where the mutual coupling is taken into account. The proposed hybrid algorithm outperforms the conventional GA with random initialization.

A novel sparse MIMO radar is presented for high-resolution single snapshot DOA estimation. Both transmit and receive arrays are divided into two uniform arrays

with increased inter-element spacings to generate two uniform sparse virtual arrays. Since virtual arrays are uniform, conventional spatial smoothing can be applied for temporal correlation suppression among sources. Afterwards, the spatially smoothed virtual arrays satisfy the co-primality concept to avoid DOA ambiguities. Physical antenna effects are incorporated in the received signal model and their effects on the DOA estimation performance are investigated.

Keywords: 5G, base station antenna (BSA), direction-of-arrival (DOA) estimation, grating lobe, MIMO radar, multi-user (MU) MIMO, multipath channel, mutual coupling, network theory, sparse array.

Preface

This thesis is in partial fulfillment for the degree of Doctor of Philosophy at Chalmers University of Technology, Gothenburg, Sweden.

The work resulting in this thesis was carried out between February 2017 and October 2021 at the Communication and Antenna Systems Group, Department of Electrical Engineering, Chalmers University of Technology. Associate Professor Rob Maaskant is the main supervisor, as well as the examiner. In addition, Professor Marianna V. Ivashina is the co-supervisor.

This project has received funding from the European Union's Horizon 2020 research and innovation programme under the Marie Sklodowska-Curie grant agreement No 721732.

Acknowledgment

Hereby, I would like to thank everyone who has supported me to accomplish this mission successfully.

First, I wish to deliver my sincere thanks to my main supervisor, Associate Professor Rob Maaskant, for his constructive criticism, patience and commitment to fundamental Electromagnetics. I would like to thank my co-supervisor Professor Marianna V. Ivashina for all the fruitful discussions and consultations. My sincere appreciation to Associate Professor Andrés Alayón Glazunov for his kind co-supervision during the first two years of my PhD study. I would like to ask Professor Bart Smolders and Assistant Professor Ulf Johannsen to accept my deepest gratitude for the brilliant comments I received from them.

I wish to thank all colleagues at the Electrical Engineering Department of Chalmers University of Technology, especially my friends at the Communication and Antenna Systems group for the wonderful, friendly and supportive work environment.

I would like to take this opportunity to thank the Netherlands Institute for Radio Astronomy (ASTRON) for hosting my three-month internship, in particular ir. Wim Van Cappellen for all the scientific discussions we had. I also wish to thank NXP Semiconductors, Eindhoven, for hosting my eighteen-month industrial secondment, especially Dr. Alessio Filippi and Dr. Venkat Roy for the joyful collaboration.

Thank you my Iranian friends, in and around Chalmers, for being my family here and also for all those laughs during Fikas.

Thank you my colleagues and friends at the SILIKA project for the joyful discussions and collaborations. I am proud of being part of this amazing project.

My sincere gratitude to my dear friend Gholam Hasan Maleki, who was my mentor for the M.Sc. entrance examination. Hasan, I never forget the trust you put in me. I truly appreciate all the guidance and support you shared with me to start this journey.

My deepest gratitude to my role models and biggest supporters in all life steps. Baba and Omid, words cannot express the feelings I have for you! I wish you could see this thesis.

To my lovely family and dear friends, thank you from the bottom of my heart, for all your support, encouragement and eternal love.

Navid,
Gothenburg, October 2021

List of Publications

This thesis is based on the work contained in the following appended papers:

Paper A
N. Amani, A. A. Glazunov, M. V. Ivashina, and R. Maaskant, "Per-Antenna Power Distribution of a Zero-Forcing Beamformed ULA in Pure LOS MU-MIMO," *IEEE Communication Letters*, vol. 22, no. 12, pp. 2515–2518, 2018.

Paper B
N. Amani, R. Maaskant, A. A. Glazunov, and M. V. Ivashina, "Network Model of a 5G MIMO Base Station Antenna in a Downlink Multi-User Scenario," in *Proceedings of the* 12^{th} *European Conference on Antennas and Propagation (EuCAP)*, London, UK, 9-13 April 2018.

Paper C
N. Amani, H. Wymeersch, U. Johannsen, A. B. Smolders, M. V. Ivashina, and R. Maaskant, "Multi-Panel Sparse Base Station Design with Physical Antenna Effects in Massive MU-MIMO," *IEEE Transactions on Vehicular Technologies*, vol. 69, no. 6, pp. 6500–6510, 2020.

Paper D
N.Amani, A. Farsaei, U. Gustavsson, T. Eriksson, F. M. J. Willems, M. V. Ivashina, and R. Maaskant, "Array Configuration Effect on the Spatial Correlation of MU-MIMO Channels in NLoS Environments," in *Proceedings of the* 14^{th} *European Conference on Antennas and Propagation (EuCAP)*, Copenhagen, Denmark, 15-20 March 2020.

Paper E
N.Amani, A. Farsaei, S. Rezaei Aghdam, T. Eriksson, M. V. Ivashina, and R. Maaskant, "Sparse Array Synthesis Including Mutual Coupling for MU-MIMO Average Capacity Maximization," resubmitted to *IEEE Transactions on Antennas and Propagation*, 2021.

Paper F
N.Amani, F. Jansen, A. Filippi, M. V. Ivashina, and R. Maaskant, "Sparse Automotive MIMO Radar for Super-Resolution Single Snapshot DoA Estimation with Mutual Coupling," resubmitted to *IEEE Access*, 2021.

Other related publications of the Author not included in this thesis:

- N. Amani, A. Filippi, and F. Jansen, "Radar Apparatus and Method," US Patent App. 16/888139, 2020.
- N. Amani, C. Bencivenni, A. A. Glazunov, M. V. Ivashina, and R. Maaskant, "MIMO Channel Capacity Gains in mm-Wave LOS Systems with Irregular Sparse Array Antennas," in *Proceedings of the IEEE-APS Topical Conference on Antennas and Propagation in Wireless Communications (APWC)*, Verona, Italy, 11–15 September 2017.
- N. Amani, R. Maaskant, and W. A. Van Cappellen, "On the Sparsity and Aperiodicity of a Base Station Antenna Array in a Downlink MU-MIMO Scenario," in *Proceedings of the International Symposium on Antennas and Propagation (ISAP)*, Busan, South Korea, 23–26 October 2018.
- N. Amani, H. Wymeersch, U. Johannsen, A. B. Smolders, M. V. Ivashina, and R. Maaskant, "Towards a Generic Model for MU-MIMO Analysis Including Mutual Coupling and Multipath Effects," in *Proceedings of the* 13^{th} *European Conference on Antennas and Propagation (EuCAP)*, Krakow, Poland, 31 March–5 April 2019.
- N. Amani, V. Roy, A. Filippi, and Rob Maaskant, "MIMO-Sparse Radars for Enhanced DOA Estimation of Spatio-Temporal Correlated Sources," in *Proceedings of the IEEE-APS Topical Conference on Antennas and Propagation in Wireless Communications (APWC)*, Granada, Spain, 9–13 September 2019.
- A. A. Glazunov, N. Amani, C. Bencivenni, R. Maaskant, and M. V. Ivashina, "Point-to-Point 3×3 MIMO Performance Gains with Aperiodic Sparse Arrays in Pure LOS Channels," in *Proceedings of the International Symposium on Antennas and Propagation (ISAP)*, Phuket, Thailand, 30 October–2 November 2017.
- A. A. Glazunov, N. Amani, A. Uz Zaman, M. V. Ivashina, and R. Maaskant, "Capacity Gains of $(3 \times 3) \times (3 \times 3)$ MIMO Fixed Links with Planar Aperiodic Sparse Arrays in Pure-LOS Channels," in *Proceedings of the* 8^{th} *IEEE-APS Topical Conference on Antennas and Propagation in Wireless Communications (APWC)*, Cartagena de Indias, Colombia, 10–14 September 2018.
- A. Farsaei, N. Amani, A. Alvarado, F. M. J. Willems, U. Gustavsson, and R. Maaskant, "On the Outage Performance of Line-of-Sight Massive MIMO with a Fixed-Length Uniform Linear Sparse Array," in *Proceedings of the IEEE-APS Topical Conference on Antennas and Propagation in Wireless Communications (APWC)*, Granada, Spain, 9–13 September 2019.

- A. Farsaei, N. Amani, R. Maaskant, U. Gustavsson, A. Alvarado, and F. M. J. Willems, "Uniform Linear Arrays with Optimized Inter-Element Spacing for LOS Massive MIMO," *IEEE Communication Letters*, vol. 25, no. 2, pp. 613–616, 2021.

Acronyms

2D	Two Dimensional
3D	Three Dimensional
3GPP	3rd Generation Partnership Project
4G	Fourth Generation
5G	Fifth Generation
AAS	Advanced Antenna System
ADAS	Advanced Driver Assistant System
AF	Array Factor
BSA	Base Station Antenna
CAGR	Compound Annual Growth Rate
CB	Conjugate Beamforming
CDF	Cumulative Distribution Function
COS	Cluster of Scatterers
CSI	Channel State Information
DOA	Direction of Arrival
DOF	Degrees of Freedom
EEP	Embedded Element Pattern
EIRP	Effective Isotropic Radiated Power
EM	Electromagnetic
EVD	Eigenvalue Decomposition
FD	Fraunhofer Distance
FOV	Field of View
GA	Genetic Algorithm
Gbps	Giga-bit-per-second
GEO	Geosynchronous Equatorial Orbit
HPBW	Half Power Beamwidth
i.i.d.	Independent and Identically Distributed
ISA	Irregular Sparse Array
LOS	Line-of-Sight
MIMO	Multiple-Input Multiple-Output

MRA	Minimum Redundancy Array
MRC	Maximum Ratio Combining
MRI	Magnetic Resonance Imaging
MRT	Maximum Ratio Transmission
MU	Multi-User
MUSIC	Multiple Signal Classification
NF	Noise Figure
UE	User Equipment
NLOS	Non-Line-of-Sight
NR	New Radio
PA	Power Amplifier
PAPC	Power Amplifier Power Consumption
RF	Radio Frequency
RIMP	Rich Isotropic Multipath
RX	Receiver
SA	Simulated Annealing
SATCOM	Satellite Communication
SDMA	Space Division Multiple Access
SF	Sparsity Factor
SINR	Signal-to-Interference-Plus-Noise Ratio
SKAI	Square Kilometer Array Interferometer
SLL	Side-Lobe-Level
SNR	Signal-to-Noise Ratio
SR	Sum-Rate
SVD	Singular Value Decomposition
TX	Transmitter
UE	User Equipment
ULA	Uniform Linear Array
ZF	Zero Forcing

Contents

Part I

Introductory Chapters

Chapter 1

Introduction

Lifestyle of human beings from education and business to communication and entertainment is becoming more and more dependent on ubiquitous internet access, all around the world. We have particularly witnessed this during the COVID-19 pandemic. Given these circumstances, the number of fixed and mobile internet-enabled devices will be constantly increasing per year. Fig. 1.1 demonstrates an estimate of the annual growth rate of different devices from 2017 to 2022, predicted by Cisco [1]. In order to provide high-quality services, there is an inevitable tendency toward higher frequencies [2]. Abundant publications from academia on this topic and novel products with promising functionalities by high-tech pioneer companies are heralding a new era of mm-wave technology.

Recent advances in integration and packaging techniques have enabled mm-wave deployment for both communication and radar applications. Thanks to the smaller wavelength, devices with reduced form factors are realizable for high-speed wireless communications [3]. In the automotive market, mm-wave radars perform high-resolution distance, speed and angle estimation [4]. However, based on Friis equation one could expect greater free-space path loss at higher frequencies under the assumption of unity gain antennas. The limited output power of highly linear and efficient solid-state circuits at mm-wave frequencies restrains the capability of transmitters to cope with the path loss. In addition, environmental effects such as gaseous absorption, precipitation and foliage loss could be critical at higher frequencies, as depicted in Fig. 1.2 [5]. Due to smaller wavelengths at mm-wave frequencies, diffraction is less pronounced compared to sub 6-GHz frequencies [6]. Hence, reflection and scattering are dominant propagation phenomena, which requires new channel models. Taking the aforementioned challenges into account, in order to benefit from the available spectrum at mm-wave frequencies, careful considerations are necessitated, which is an emerging area of research.

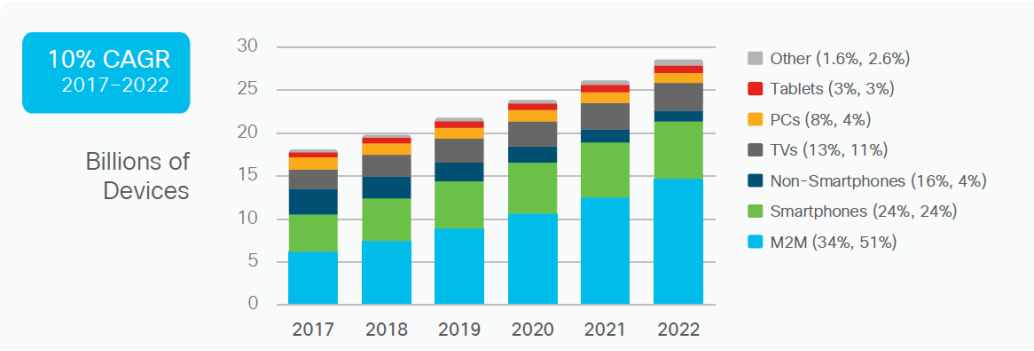

Figure 1.1: Global devices and connections growth [1]. CAGR stands for compound annual growth rate.

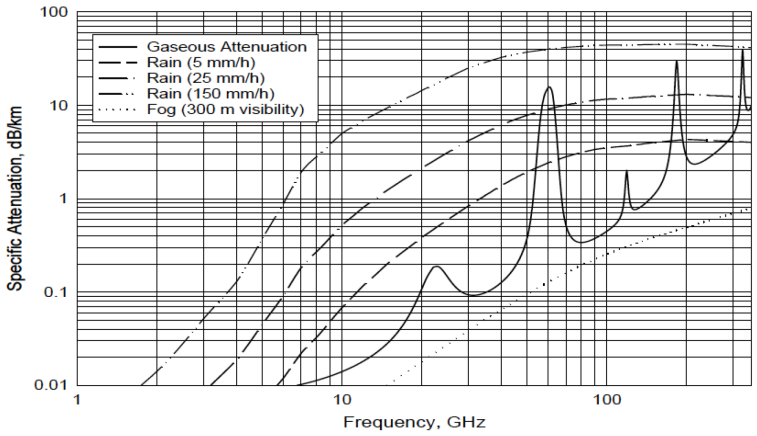

Figure 1.2: Atmospheric attenuation versus frequency [5].

1.1 mm-wave Frequencies for Wireless Communication

The demand for larger wireless bandwidth is incessantly increasing and fourth-generation (4G) technologies are on the verge of reaching their limits. In order to provide multi-gigabit-per-second (Gbps) wireless transmission, mm-wave technology is proposed for the next generation of wireless communication, known as fifth-generation (5G). However, due to the higher losses at mm-wave frequencies, an omni-directional transmission, illustrated in Fig. 1.3 (a) [3], is not a feasible approach. Directive communication, as shown in Fig. 1.3 (b) [3], is envisioned to overcome the path loss and to satisfy the required effective isotropic radiated power (EIRP). The idea of massive multiple-input multiple-output (MIMO) and its intriguing properties to serve multiple simultaneous users have been released in 2010 [7]. It has attracted the attention of many scholars in both academia and industry. Spatial division multiple access

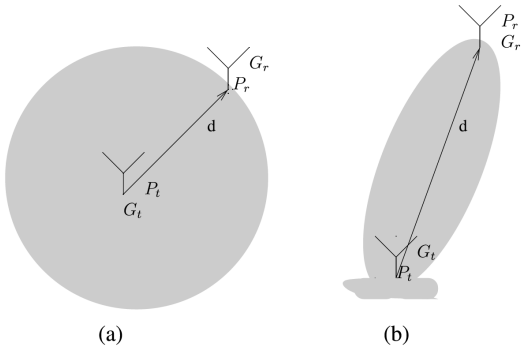

Figure 1.3: (a) Omni-directional transmission, (b) directional transmission [3].

(SDMA) technique enables serving multiple users at the same time and frequency [8]. Although one can benefit from increasing the number of antennas at the base station to generate narrow beams, this also arises many practical challenges when it comes to fabrication. A real massive MIMO implementation is hindered by high system complexity and hardware energy consumption. As it is noted in [9], the routing of circuit components and integration of antennas becomes cumbersome within a single panel for a large number of elements. An effective thermal management in a dense array is required due to the relatively low efficiency of power amplifiers (PAs) at mm-wave frequencies [10]. Regarding the latency of the system, the complexity of the signal processing algorithms scales up with the number of elements. Furthermore, the effect of mutual coupling at the base station antenna (BSA) needs to be taken into account carefully when spatial multiplexing is applied since the BSA gain pattern variation causes a sum-rate loss in the system [11]. Hence, in contrast to classical uniform arrays, spreading a given number of antennas in a novel and unconventional fashion to keep the system complexity manageable and maintain/enhance the system performance is of huge interest for 5G applications.

1.2 mm-wave Frequencies for Automotive Radar

Another aspect of mm-wave technology which contributes to human safety and comfort is automotive radar. The development of mm-wave semiconductor technology along with signal processing algorithms are the backbone of the new generation of automotive radars. They contribute to the advanced driver assistant system (ADAS) for detection of objects, their speed and location. Direction of arrival (DOA) estimation as one of the radar tasks is critical to distinguish targets in one range-velocity bin. Better angular resolution is vital to distinguish closely spaced targets. The radar angular resolution using Rayleigh criterion is defined as [12]:

$$\Delta\varphi = 1.22\frac{\lambda}{A}, \tag{1.1}$$

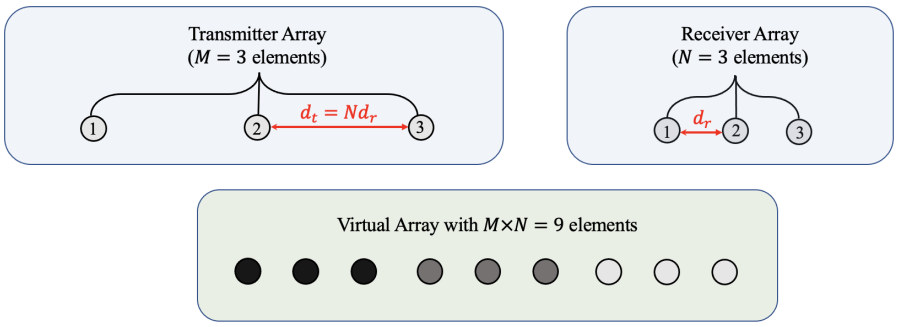

Figure 1.4: MIMO radar configuration. Both transmitter and receiver arrays have three elements in this example.

where λ is a wavelength and A is the antenna aperture size. The larger the antenna aperture, the better the radar angular resolution. This can be accomplished by either increasing the number of antennas or enlarging the element spacing. The former increases the complexity of the system while the latter, for spacings larger than half-wavelength, suffer from spatial under-sampling known as aliasing.

MIMO technology and its benefits have been widely deployed for communication applications through the years. A similar technique has appeared in the radar literature [13, 14] to enhance radar performance by virtually extending its aperture size. The concept of MIMO radar is depicted in Fig. 1.4, where waveform orthogonality and matched filtering are deployed at the transmitter and receiver arrays, respectively. A transmitter array with M antennas and a receiver array with N antennas generates a virtual MIMO array with $M \times N$ elements. This dramatically enhances the radar performance by occupying a larger aperture with more elements.

Another approach to increase the aperture dimension with a given number of antennas, while the effects of grating lobes or aliasing are suppressed, is the use of non-uniform arrays. The first type of non-uniform arrays to maximize the resolution by minimizing the number of redundant spacing is minimum-redundancy array (MRA) [15]. Other types of nun-uniform/unconventional arrays have already been proposed to enhance the resolution, specifically for radar applications, e.g., co-prime arrays [16]. Therefore, it is evident that a smart distribution of a given number of antennas in a sparse manner, rather than uniform arrays, renders unique advantages.

1.3 Research Questions

The focus of this thesis is to propose novel sparse array architectures for 5G base station and automotive radar applications which improve the respective performance metrics and relaxes implementation complexities. The research questions which are addressed in this thesis, classified in two categories depending on the application, can

be summarized as follows:

1.3.1 Wireless Communication

- In a multi-user (MU) MIMO scenario, the BSA should be seen as a part of the whole system. Therefore conventional antenna pattern metrics, e.g., the side-lobe-level (SLL) and the half-power beamwidth (HPBW), would not be sufficient metrics to evaluate the system performance. Furthermore, sparse array topologies have been reported superior in comparison to their conventional counterparts in earlier studies [17], [18]. Hence, the first question arises as: *Could there be any advantage in the end-performance of a MU-MIMO system by means of employing a sparse BSA array?*

- Bearing in mind that a 5G BSA design requires knowledge of electromagnetics (EM), array signal processing, and wireless communication, a system-level simulator needs to be developed. Hence, the second question is: *How to develop a unified MU-MIMO simulation platform which incorporates both antenna and channel effects while it is suitable for signal processing purposes?*

- Upon a quick web search on "*Massive MIMO*" or "*MU-MIMO*", it can be figured out that most contributions in these areas have been made in the "*Wireless Community*", where detrimental/non-ideal antenna effects are typically underestimated. The common assumptions in their analyses are to employ isotropic radiators and to neglect mutual coupling effects. So, *What would be the impact of physical antenna effects, such as gain pattern variation and mutual coupling effects, on the performance of a MU-MIMO system?*

1.3.2 Automotive Radar

- Due to the vehicle speed, there are specific requirements for successful DOA estimation by automotive radars. The most critical challenge is the lack of snapshots (one radar measurement cycle). Commonly in the literature, uncorrelated targets are identified by non-uniform radars using a large number of snapshots, which seems to be impractical. So, the question is: *can there be any advantage in deploying non-uniform arrays in automotive radars for the DOA estimation of correlated sources?*

- Sparse signal recovery algorithms are proposed for fine angular resolution by sparse sensor arrays. However, these algorithms are based on iterative or probabilistic approaches. Hence, they are considered computationally heavy for real-time processing. The second question is: *how to perform DOA estimation by a non-uniform sensor array using conventional signal processing algorithms,*

which are well developed for uniform arrays, e.g., spatial smoothing [19] and fast Fourier transform (FFT) methods?

- Finally, *how to incorporate physical antenna effects such as mutual coupling in the signal model for the DOA estimation problem?*

1.4 Thesis Outline

This thesis is organized in two main parts. The first part of this thesis summarizes the fundamentals of antenna arrays and the background of the problem, ordered in six chapters. This provides a vivid picture and perception of the author's papers, which are appended in the second part. Non-appended publications can be found in the section "*List of Publications*".

Regarding part I, Chapter 1 introduces the thesis, the background of the problem and the research questions which are addressed in conjunction with the thesis outline. Antenna arrays, beamforming, MIMO antennas, MU-MIMO systems and relevant network theory are reviewed in Chapter 2. The benefits of sparse arrays in other application areas, their drawbacks and potential solutions to tackle them are proposed in Chapter 3. Since this thesis is focused on the application of sparse arrays for 5G communication and automotive radars, they are discussed in the separate Chapters 4 and 5. In Chapter 4, a MU-MIMO system is introduced. The inter-user spatial correlation is defined as a critical metric which determines the distinguishability of multiple users in the spatial domain. Afterwards, several optimization based sparse array syntheses for 5G BSA design are reviewed. The fundamentals of DOA estimation is discussed in Chapter 5. The multiple signal classification (MUSIC) algorithm and spatial smoothing technique are briefly explained. Furthermore, recently proposed sparse array topologies, e.g., co-prime and nested arrays, for enhanced DOA estimation are studied. Finally, Chapter 6 concludes this thesis with a summary and proposes suggestions for possible future research directions.

Part II of this thesis includes the most relevant publications of the author in the form of six appended papers. Paper A is analytically investigating the antenna port power variation across a uniform linear array (ULA) as a function of angular separation between two users while the zero forcing (ZF) precoder is applied. Papers B and C propose the network theoretical model to incorporate both physical antenna and channel effects. A co-simulation platform is proposed and based on that a multi-panel sparse BSA is suggested. Paper D proposes an electromagnetic modeling of a NLOS channel, where scatterers are considered as resonant dipoles. It is shown that an aperiodic distribution of a given number of antennas into the sparse aperture is beneficial for correlation suppression among randomly located users. A two-phase optimization framework to find an irregular sparse array distribution which outperforms its regular counterpart in terms of average capacity in a MU-MIMO system is

presented in Paper E. Paper F demonstrates superior performance of a novel sparse MIMO radar for high-resolution single snapshot DOA estimation. Mutual coupling and its effects on the DOA estimation performance are scrutinized in this paper as well.

Chapter 2

Theoretical Background

Usually, the radiation pattern of a single antenna array element is relatively wide as it does not provide high directivity. For many applications, e.g., serving multiple users by the SDMA technique in 5G communication and distinguishing spatially correlated targets in automotive radars, high directivity is a must. This can be achieved by enlarging the electrical size of the antenna. Another way to enhance the directivity is to deploy array antennas consisting of several elements. The superposition of radiation characteristics of several antenna elements in the far-field region leads to high directivity. Another appealing aspect of array antennas is the ability to generate different radiation patterns by changing the excitation (amplitude and phase) of their individual elements. This is known as beamforming or more generally pattern shaping. In this chapter, the theory of antenna arrays and their use cases are briefly reviewed.

2.1 Linear Arrays

For simplicity, we start with a linear array of equally spaced individually excited elements, shown in Fig. 2.1. Mutual coupling is ignored in this section. The array is comprised of M elements with a constant inter-element spacing of d. The individual element excitation is denoted by a_m, where m represents the element index ($m = 1, 2, \ldots, M$). Assuming that $\angle a_m = -\phi_m$, the complex element excitation can be written as $a_m = \mid a_m \mid e^{-j\phi_m}$. The angle from the broadside direction of the array is denoted by θ. Under the assumption of similar performance by individual elements, the far-field function of the whole array is a single element far-field function $\mathbf{G}(\hat{r})$ multiplied by a factor widely referred to as array factor (AF) [20, 21].

$$\mathbf{G}_A(\hat{r}) = \mathbf{G}(\hat{r}) \underbrace{\sum_{m=1}^{M} \mid a_m \mid e^{j(\beta(m-1)d\sin\theta - \phi_m)}}_{\text{AF}}, \tag{2.1}$$

where β is the wave-number.

In order to concentrate on the array performance, one could assume isotropic radiators, which reduces the array far-field function to the AF. With no amplitude tapering ($\mid a_m \mid = 1$) and no phase shift ($\phi_m = 0$) across the array aperture, the AF is

$$\text{AF} = \sum_{m=1}^{M} e^{j(m-1)\Psi} = \frac{1 - e^{jM\Psi}}{1 - e^{j\Psi}}, \tag{2.2}$$

where $\Psi = \beta d\sin\theta$. Using Euler's formula, the modulus of the array factor can be represented by

$$\mid \text{AF} \mid = \frac{\sin(M\Psi/2)}{\sin(\Psi/2)}. \tag{2.3}$$

Equation (2.3) implies that the maximum happens at $\theta = 0$ which is the broadside direction of the array. The maximum of the first side lobe with a large number of antennas happens approximately at $\Psi = 3\pi/M$ [20]. Its magnitude can be computed as

$$\text{SLL} = 20\log_{10}\left(\frac{2}{3\pi}\right) = -13.46 \text{ dB} \tag{2.4}$$

As an example, the radiation pattern of a ULA with 64 elements and $d = \lambda/2$ is plotted in Fig. 2.2.

2.1.1 Phased (Scanning) Array

It has been shown that without a phase shift between antenna elements, the main radiation of an array happens at the broadside direction. The intriguing property of a phased array is electronic scanning capability, which avoids mechanical rotation. A constant phase progression between elements enables beam scanning. In order to steer the beam at direction θ_s, the following phase difference between adjacent elements is required:

$$\Delta\phi = \frac{2\pi d\sin\theta_s}{\lambda} \tag{2.5}$$

For the example in Fig. 2.2, in order to put the main beam at 60° the required phase progression based on (2.5) is $\Delta\phi = \sqrt{3}\pi/2$. The radiation pattern with $\sqrt{3}\pi/2$ phase progression is shown in Fig. 2.3. A drawback of electronic beam scanning is beam

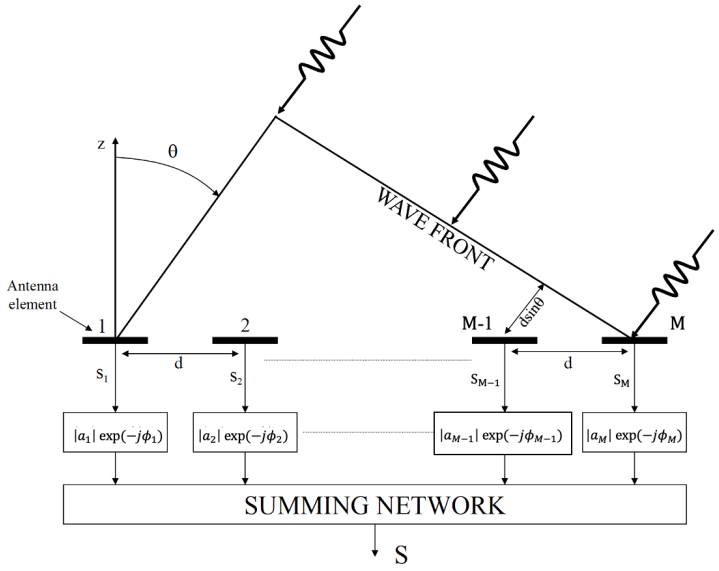

Figure 2.1: Uniform linear array (ULA) of individually excited elements [22].

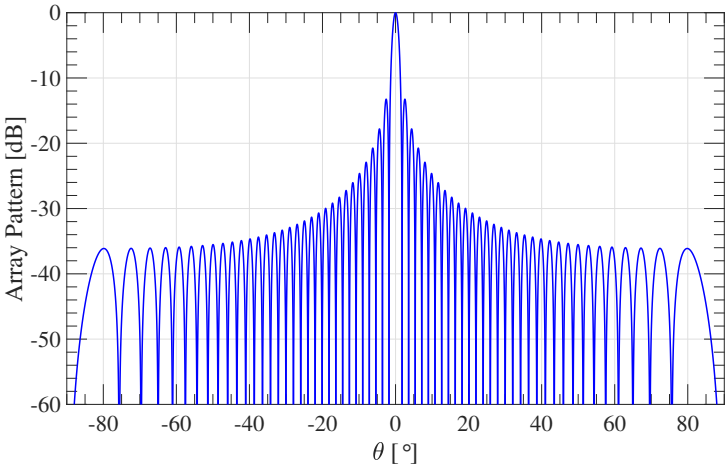

Figure 2.2: Radiation pattern of a ULA with 64 elements and $d = \lambda/2$.

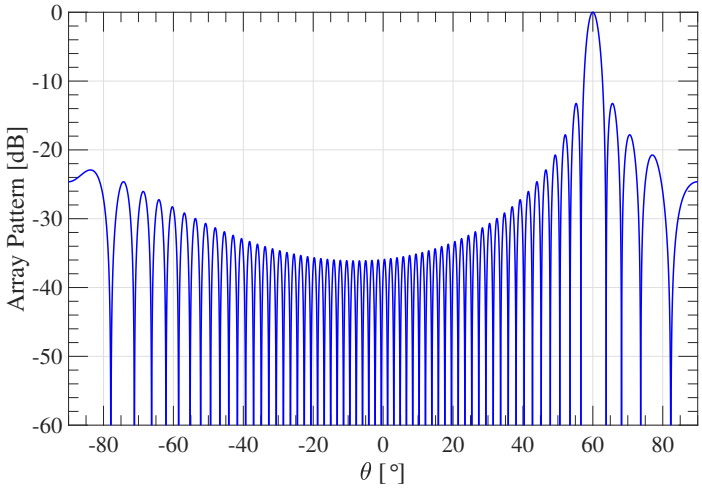

Figure 2.3: Beam scanning at 60° using a ULA with 64 elements and $d = \lambda/2$.

broadening. That is, the main beam widens while it steers off-broadside. The beam broadening can be quantified by the HPBW and the following expression

$$\mathrm{HPBW}_{\theta_s} = \frac{\mathrm{HPBW}_{\theta_0}}{\cos\theta_s}. \tag{2.6}$$

So, at $\theta_s = 60°$ the HPBW is twice that of the broadside direction.

When electronic scanning is applied, other maxima or replicas of the main beam can happen inside the visible region, which is undesirable. These are traditionally called grating lobes. To avoid this issue, careful considerations are required regarding the inter-element spacing and the scan angle θ_s. Maximum inter-element spacing ($d_{\max}$) to achieve a grating lobe-free radiation pattern depends on the scan angle and can be calculated by:

$$d_{\max} < \frac{\lambda}{1 + |\sin\theta_s|} \tag{2.7}$$

For the example in Fig. 2.2, assuming that $\theta_s = \pm\pi/2$, the maximum inter-element spacing is

$$d_{\max} < \frac{\lambda}{2} \tag{2.8}$$

The radiation pattern in the case that the main beam is steered at $\theta_s = \pi/2$ is plotted in Fig. 2.4. The appearance of a grating lobe at $\theta = -\pi/2$ is clear.

2.1.2 Amplitude Tapering

The beam scanning capability with uniform amplitude tapering and constant phase progression has been illustrated. However, for some applications, e.g., military communication, space observation, biomedical imaging and radar systems, low SLL is

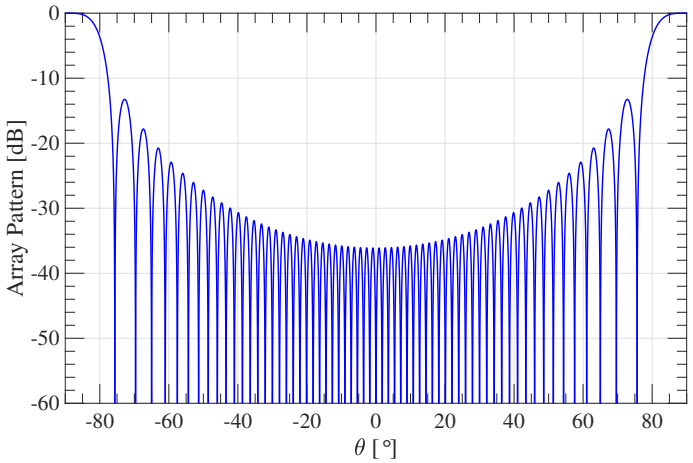

Figure 2.4: Beam scanning at 90° using a ULA with 64 elements and $d = \lambda/2$.

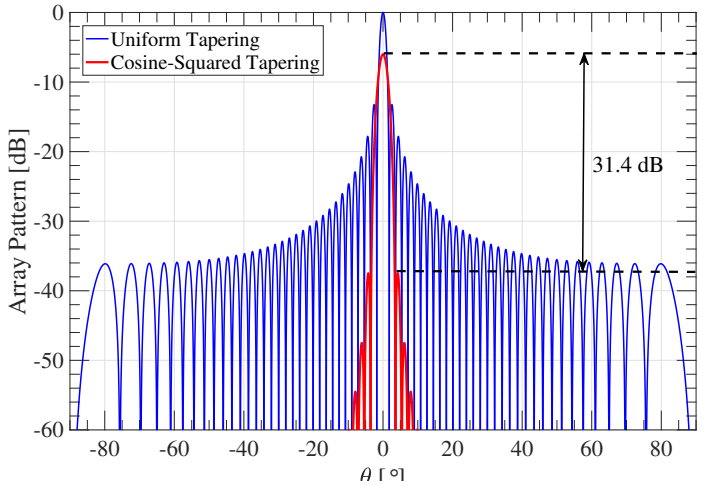

Figure 2.5: Radiation pattern of a ULA with 64 elements and $d = \lambda/2$ with uniform and cosine-squared amplitude tapering.

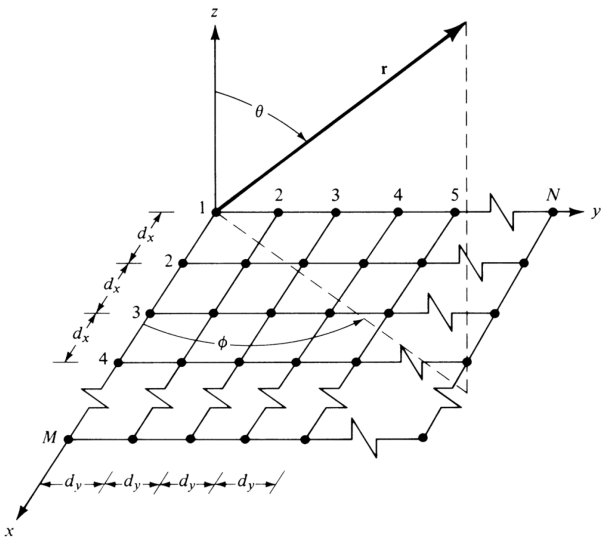

Figure 2.6: Planar array geometry [20].

a must to avoid interference. Amplitude tapering is a simple approach to suppress the SLL. Binomial, Dolph-Tschebycheff, Taylor and cosine-squared are some known tapering approaches among many.

A comparison between two radiation patterns in Fig. 2.5 demonstrates a significant SLL reduction. However, beam broadening and directivity reduction appear when amplitude tapering is employed. So, the major shortcoming of the amplitude tapering is the aperture (or taper) efficiency reduction. This can be quantified by the following expression [23].

$$\eta_{tap} = \frac{\left| \sum_{m=1}^{M} a_m \right|^2}{M \sum_{m=1}^{M} |a_m|^2} \tag{2.9}$$

2.2 Planar Arrays

For beam scanning in three dimensional (3D) space, planar arrays are needed. Using a similar analysis as in the previous section, the normalized array factor with uniform amplitude and zero phase progression is

$$| \text{ AF } | = \frac{\sin\left(M\Psi_x/2\right)}{\sin\left(\Psi_x/2\right)} \times \frac{\sin\left(N\Psi_y/2\right)}{\sin\left(\Psi_y/2\right)}, \tag{2.10}$$

where $\Psi_x = \beta d_x \sin\theta\cos\phi$ and $\Psi_y = \beta d_y \sin\theta\sin\phi$. Fig. 2.7 illustrates the location of the main lobe and grating lobes of a planar array with uniform spacing [21]. A rectangular uv-coordinate system with $u = \sin\theta\cos\phi$ and $v = \sin\theta\sin\phi$ are used. As can

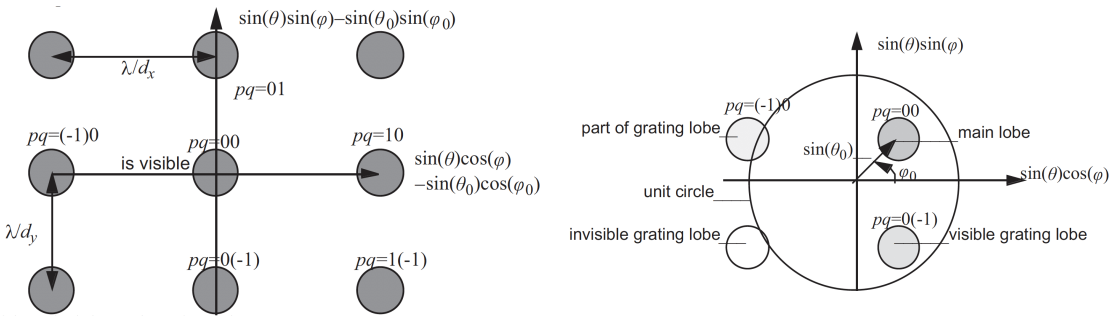

Figure 2.7: (left) Array factor showing the location of the main and grating lobes; (right) combined array and element factors [21].

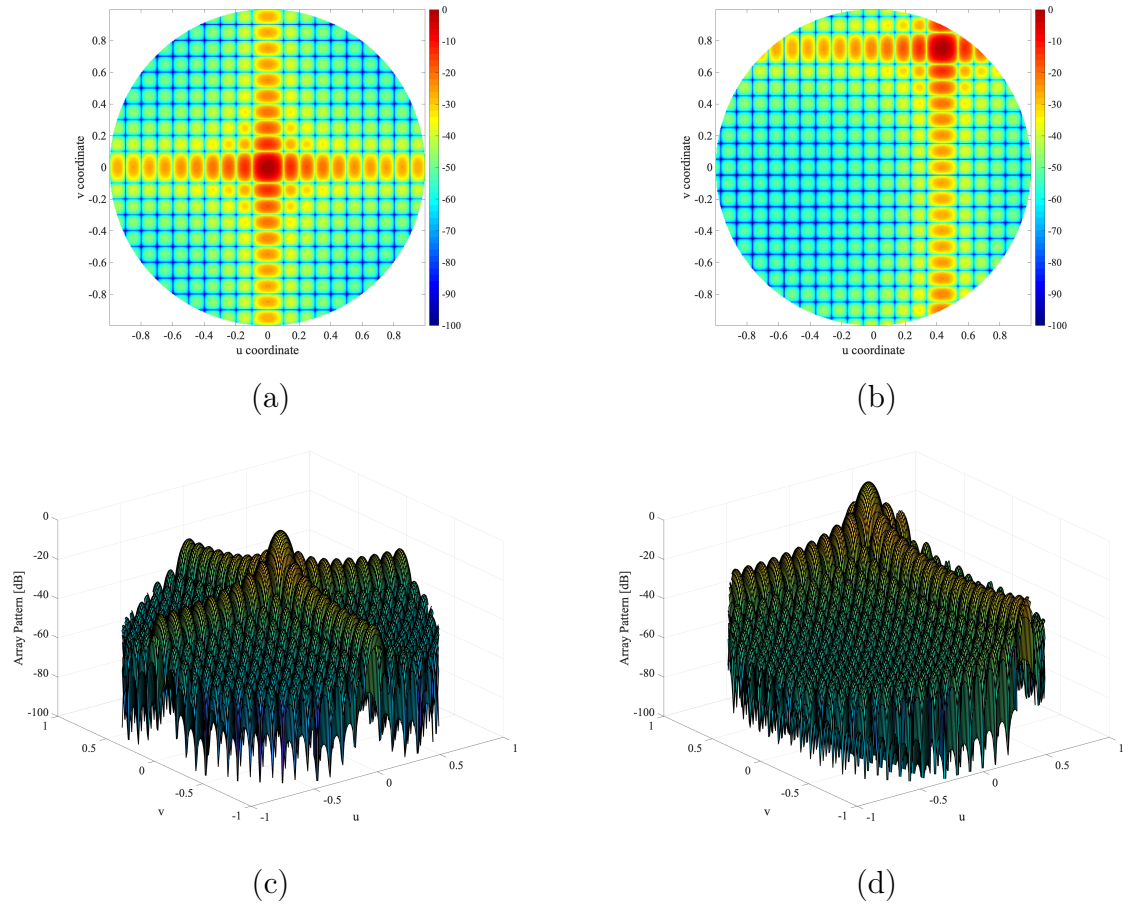

Figure 2.8: Planar array radiation patterns with uniform amplitude tapering: (a) and (c) broadside direction, (b) and (d) scanned beam at $\theta_s = 60°$ and $\phi_s = 60°$.

be noticed, increasing the inter-element spacing (d_x or d_y) in a uniform array reduces the distance between the main beam and grating lobes, which may consequently bring the grating lobes into the visible region.

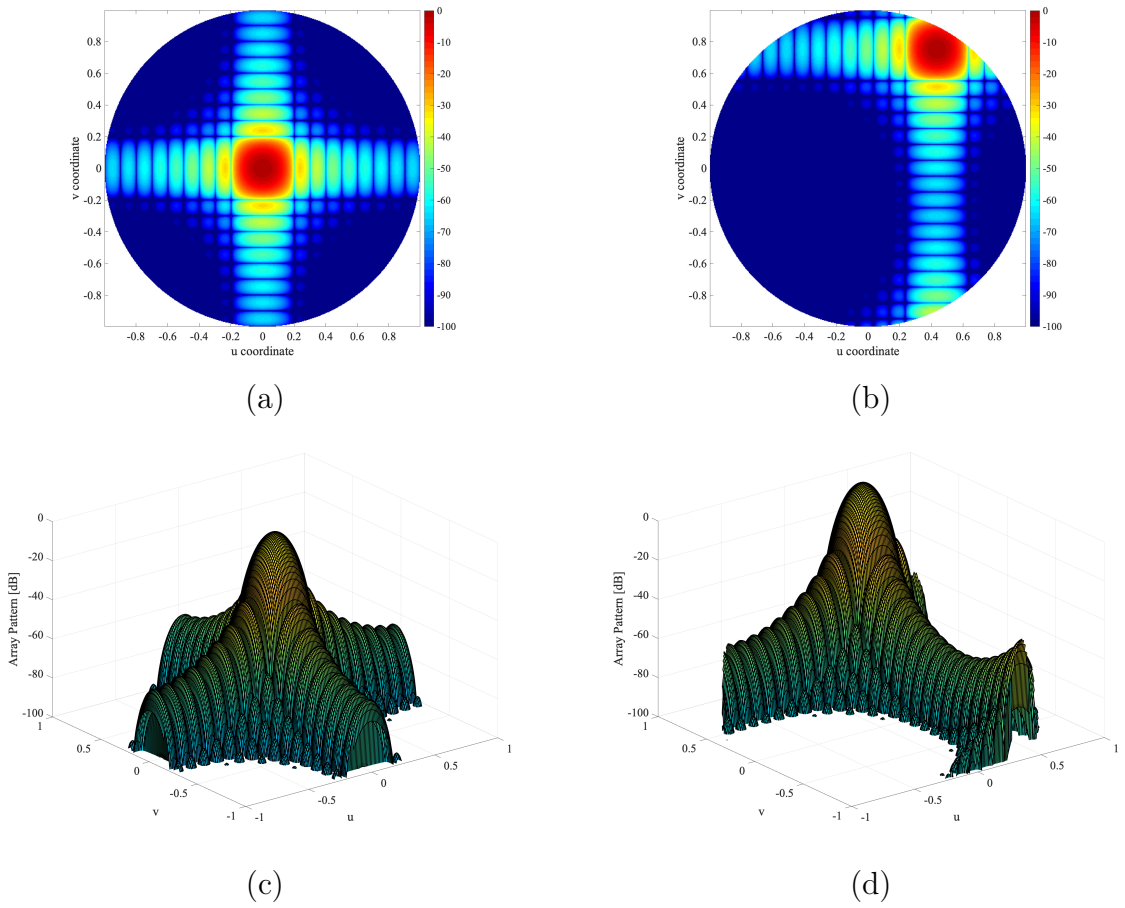

Figure 2.9: Planar array radiation patterns with cosine-squared tapering: (a) and (c) broadside direction, (b) and (d) scanned beam at $\theta_s = 60°$ and $\phi_s = 60°$

Similar to linear arrays, phase progression and amplitude tapering can be used for beam steering and SLL reduction. As an illustration, a 20×20 planar array with $d_x = d_y = 0.5\lambda$ is assumed. The radiation patterns for the broadside direction and scanned beam at $\theta_s = 60°$ and $\phi_s = 60°$ are plotted in Fig. 2.8. The same radiation patterns are extracted in Fig. 2.9 when cosine-squared tapering is applied. A remarkable SLL reduction is observed, however, beam broadening is obvious as well.

2.3 Mutual Coupling

So far, there was no interaction between antenna elements inside an array and the element patterns were assumed to be identical. Nonetheless, in reality antennas in the proximity of other antennas or objects cannot be assumed isolated. That is due to the induced current by the near-field of an antenna element. The mutual interaction be-

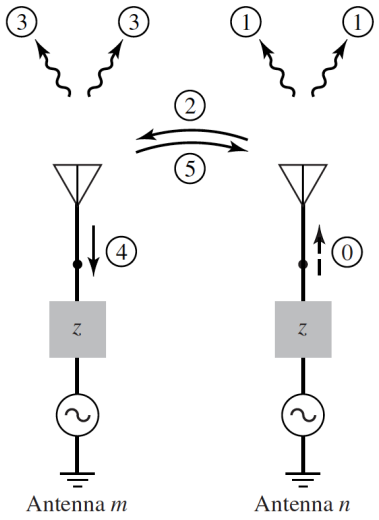

Figure 2.10: Mutual coupling between two antenna elements in the transmitting mode [20].

tween antennas in an array is called mutual coupling. This effect changes the current distribution on the antenna and varies its radiation characteristics. Furthermore, the input impedance of an antenna element deviates from its isolated counterpart and can cause an impedance mismatch at the antenna input.

The deviation of the antenna input impedance from its isolated one is commonly called active/scan impedance. It is critical in the case of beamforming since scan blindness may happen [21]. The scan impedance is formulated as [21]:

$$Z_m^{\text{scan}} = \sum_{n=1}^{N} Z_{mn} \left(\frac{I_n}{I_m} \right), \tag{2.11}$$

where Z_{mn} is the mutual impedance between antennas m and n with current excitation of I_m and I_n, respectively. The mismatch loss due to the active/scan impedance can be measured by the so-called decoupling efficiency [24, 25], as below:

$$\eta_{\text{decoup}} = \frac{\sum_{m=1}^{M} P_{\text{acc},m}}{\sum_{m=1}^{M} \frac{P_{\text{acc},m}}{(1 - |\Gamma_m|^2)}}, \tag{2.12}$$

where $P_{\text{acc},m}$ and Γ_m represent the accepted power and active reflection coefficient at each antenna port m, respectively.

The induced current on the neighbouring element by the fields of the excited one perturbs the isolated element pattern. The adjusted element pattern due to the driven neighbouring element in an array is known as embedded element pattern (EEP). The

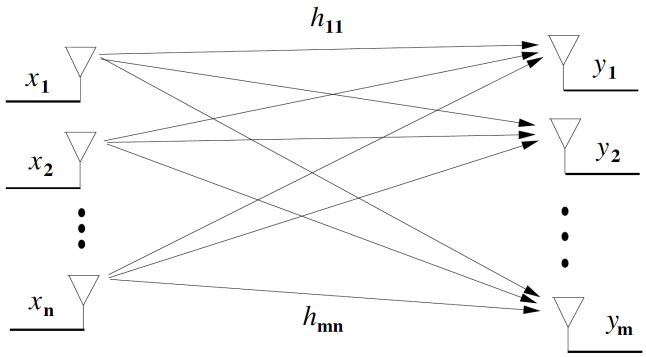

Figure 2.11: A MIMO system with n transmit and m receive antennas [28].

EEPs for the edge elements can be different from the elements in the interior of the array since edge elements have fewer elements at their proximity. Different loading conditions can be applied on non-driven element terminals such as open circuit, short circuit and match terminated when the driven terminal is excited by a source current, a source voltage or an incident wave, respectively [26].

2.4 MIMO Antennas

A communication signal is being highly affected by fading in a multipath environment [27, 28]. In order to enhance the reliability of a wireless link, diversity schemes can be deployed. The idea is to transmit the same information (single data stream) through several paths [27, 28]. For instance, a maximum ratio combiner adds several received signals coherently to increase the ultimate signal-to-noise ratio (SNR), which is known as diversity gain.

Multiple transmit and multiple receive antennas, i.e., a MIMO channel, can also increase the capacity by spatially multiplexing several data streams [29, 30]. A schematic representation of a MIMO system is shown in Fig. 2.11. A MIMO system can be described by [27]:

$$\begin{bmatrix} y_1 \\ y_2 \\ \vdots \\ y_m \end{bmatrix} = \begin{bmatrix} h_{11} & \cdots & h_{1n} \\ \vdots & \ddots & \vdots \\ h_{m1} & \cdots & h_{mn} \end{bmatrix} \begin{bmatrix} x_1 \\ x_2 \\ \vdots \\ x_n \end{bmatrix} + \begin{bmatrix} n_1 \\ n_2 \\ \vdots \\ n_n \end{bmatrix}. \tag{2.13}$$

A compact representation of (2.13) is:

$$\mathbf{y} = \mathbf{H}\mathbf{x} + \mathbf{n}, \tag{2.14}$$

where $\mathbf{x}$, $\mathbf{y}$ and $\mathbf{n} \sim \mathcal{CN}(\mathbf{0}, N_0\mathbf{I}_m)$ are the transmitted signal, received signal and white Gaussian noise, respectively. $\mathbf{I}_m$ is an identity matrix of size m. The channel

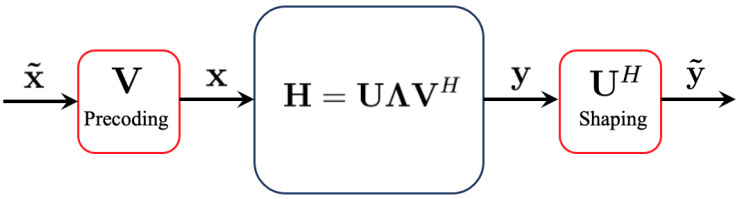

Figure 2.12: Creating parallel channels through the SVD in a MIMO system.

matrix is denoted by $\mathbf{H}$ which is assumed to be known at both the transmitter and receiver. The main idea is to create parallel independent channels. Since the channel state information is available at the transmitter, the singular value decomposition (SVD) can be applied on the channel matrix $\mathbf{H}$.

$$\mathbf{H} = \mathbf{U}\mathbf{\Lambda}\mathbf{V}^H, \tag{2.15}$$

where $\mathbf{U}$ and $\mathbf{V}$ are unitary matrices. The Hermitian operator is denoted by $(.)^H$. $\mathbf{\Lambda}$ is a rectangular matrix with non-negative real numbers as its diagonal elements, where off-diagonal elements are zero. The diagonal elements are singular values of the channel matrix $\mathbf{H}$. The rank of $\mathbf{H}$ matrix is $\mathrm{R}_{\mathbf{H}} \leq \min(\mathrm{n}, \mathrm{m})$, where n and m are the number of elements at the transmitter and receiver, respectively. With a pre-processing at the transmitter and post-processing at the receiver, as shown in Fig. 2.12, (2.14) can be rewritten as

$$\tilde{\mathbf{y}} = \mathbf{\Lambda}\tilde{\mathbf{x}} + \tilde{\mathbf{n}}, \tag{2.16}$$

where $\tilde{\mathbf{x}} = \mathbf{V}^H\mathbf{x}$, $\tilde{\mathbf{y}} = \mathbf{U}^H\mathbf{y}$ and $\tilde{\mathbf{n}} = \mathbf{U}^H\mathbf{n}$. This MIMO technique renders $\mathrm{R}_{\mathbf{H}}$ parallel channels.

2.5 Multi-User Beamforming (Precoding)

The proposed solution for 5G wireless communication is to serve multiple users at the same time and frequency resources. The MU-MIMO system, shown in Fig. 2.13, is an enabling technology that distinguishes users in the spatial domain. The SVD technique is not applicable in MU-MIMO since multiple users are spatially separated and shaping at the receiver is not possible anymore. Assuming M antennas at the base station and K users, the system model can be represented by:

$$\begin{bmatrix} y_1 \\ y_2 \\ \vdots \\ y_K \end{bmatrix} = \begin{bmatrix} \mathbf{h}_1^T \\ \mathbf{h}_2^T \\ \vdots \\ \mathbf{h}_K^T \end{bmatrix} \begin{bmatrix} \mathbf{w}_1 & \mathbf{w}_2 & \cdots & \mathbf{w}_K \end{bmatrix} \begin{bmatrix} s_1 \\ s_2 \\ \vdots \\ s_K \end{bmatrix} + \begin{bmatrix} n_1 \\ n_2 \\ \vdots \\ n_K \end{bmatrix}, \tag{2.17}$$

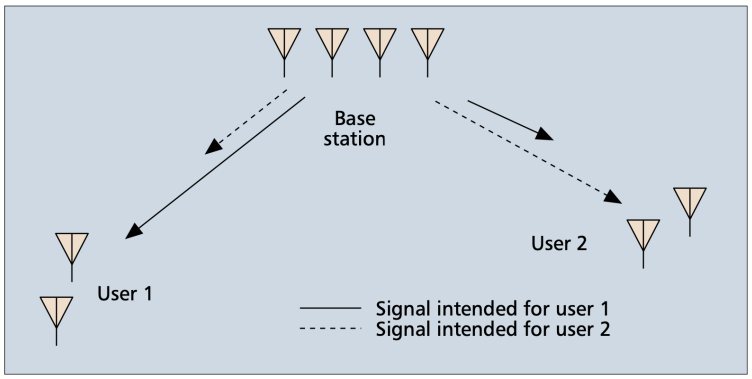

Figure 2.13: An illustration of a MU-MIMO downlink [31].

where $(.)^T$ is the transpose operation. The compact form of (2.17) is

$$\mathbf{y} = \mathbf{HWs} + \mathbf{n}, \tag{2.18}$$

where $\mathbf{y} \in \mathbb{C}^{K\times 1}$ is the received signal vector. The transmit signal vector to the UEs and the channel matrix is denoted by $\mathbf{s} \in \mathbb{C}^{K\times 1}$ and $\mathbf{H} \in \mathbb{C}^{K\times M}$, respectively. $\mathbf{W} \in \mathbb{C}^{M\times K}$ is known as the precoding/weight matrix to serve multiple UEs.

The critical challenge of such a MU-MIMO system is to shape the transmit signal vector while considering the interference of other users. Simple linear precoding algorithms, e.g., conjugate beamforming (CB) and ZF, are claimed to perform nearly as well as nonlinear precoders in massive MIMO systems [7]. The weights can be calculated by:

$$\mathbf{W} = \begin{cases} \mathbf{H}^H & \text{for CB} \\ \mathbf{H}^H(\mathbf{H}\mathbf{H}^H)^{-1} & \text{for ZF} \end{cases} \tag{2.19}$$

It is worth noting that precoding or beamforming for MU-MIMO does not necessarily mean to make directive beams, as it is known in the Antenna Community. In pure line-of-sight (LOS) environments, where there is no scatterer, the precoder at the base station forms beams toward users. However, in non-line-of-sight (NLOS) scenarios, which is expected to happen in urban environments, the multipath scatterers are being deployed for communication between the base station and the users. In the latter case, the radiation pattern is formed based on the channel matrix and we may not get any beam. Hence, pattern shaping might be more general terminology. Furthermore, classical antenna metrics such as HPBW and directivity might not be applicable for performance evaluation of the wireless link.

This is shown in Fig. 2.14 where the base station is serving two users using ZF precoder in pure LOS and NLOS environments. Blue circles represent scatterers and radiation patterns are plotted for different user locations while the scatterers are fixed. In Figs. 2.14 (a) and (b), it can be observed that in contrast to the LOS environment, where clear directive beams are created toward users, in the NLOS

case the radiation pattern is shaped irregularly in order to take advantage of the scatterers. We, therefore, do not observe two distinct beams. In Fig. 2.14 (c) it is observed that in the LOS environment if two users are located at the same angle with respect to the base station $\theta_1 = \theta_2$, singularity happens in the weight matrix calculation by the ZF beamformer. Hence, there is no data transmission. This is not happening in the NLOS scenario.

2.6 Network Theory

The advent of smart antennas and advanced antenna systems (AASs) in response to current customer demands for applications like adaptive beamforming and pattern control, real-time processing, MIMO systems, and MU communication, requires close collaboration of several disciplines. A rigorous framework which accounts for electromagnetic effects, e.g., mutual coupling and EEP, propagation aspects, e.g., multipath, fading and shadowing, and signal processing techniques is necessitated. Network theory by the aid of a multi-port network model, shown in Fig. 2.15, and network parameters can make a bridge between different disciplines [32].

The input voltage and current vectors are denoted by $\mathbf{v}_1$ and $\mathbf{i}_1$. Similarly, at the output we have $\mathbf{v}_2$ and $\mathbf{i}_2$ vectors. A linear network equation based on the impedance parameters can then be represented by

$$\begin{bmatrix} \mathbf{v}_1 \\ \mathbf{v}_2 \end{bmatrix} = \begin{bmatrix} \mathbf{Z}_{11} & \mathbf{Z}_{12} \\ \mathbf{Z}_{21} & \mathbf{Z}_{22} \end{bmatrix} \begin{bmatrix} \mathbf{i}_1 \\ \mathbf{i}_2 \end{bmatrix} \tag{2.20}$$

The self and mutual impedances at the input ports are captured by $\mathbf{Z}_{11}$. Similarly, $\mathbf{Z}_{22}$ represents the self and mutual impedances at the output ports. The mutual impedances between input and output ports are denoted by $\mathbf{Z}_{12}$ and $\mathbf{Z}_{21}$. Due to reciprocity, $\mathbf{Z}_{12} = \mathbf{Z}_{21}^T$ holds.

The relationship between the input and output voltage vectors of the network model can be extracted, using the network equation, as [33, 34]

$$\mathbf{v}_2 = \mathbf{Z}_L \left(\mathbf{Z}_L + \mathbf{Z}_{22}\right)^{-1} \mathbf{Z}_{21} \mathbf{Z}_{11}^{-1} \mathbf{v}_1, \tag{2.21}$$

where $\mathbf{Z}_L = Z_L \mathbf{I}_M$, assuming similar loading conditions for receiving antenna elements. Taking into account that transmit antennas are equipped with a source voltage $\mathrm{V_s}$ with $\mathrm{Z_s}$ intrinsic impedance, the relation between the source voltage vector $\mathbf{v}_\mathrm{s}$ and the transmit voltage vector $\mathbf{v}_1$ is

$$\mathbf{v}_1 = \mathbf{Z}_{11} \left(\mathbf{Z}_{11} + \mathbf{Z}_\mathrm{s}\right)^{-1} \mathbf{v}_\mathrm{s}, \tag{2.22}$$

where $\mathbf{v}_\mathrm{s} = [\mathrm{V_{s1}}, \mathrm{V_{s2}}, \ldots, \mathrm{V_{sM}}]^T$ and $\mathbf{Z}_\mathrm{s} = \mathrm{Z_s} \mathbf{I}_M$. Therefore, eq. (2.21) can be represented by:

$$\mathbf{v}_2 = \mathbf{Z}_L \left(\mathbf{Z}_L + \mathbf{Z}_{22}\right)^{-1} \mathbf{Z}_{21} \left(\mathbf{Z}_{11} + \mathbf{Z}_\mathrm{s}\right)^{-1} \mathbf{v}_\mathrm{s}. \tag{2.23}$$

The relation between source and received voltages in eq. (2.23) captures the physical antenna and channel effects. Furthermore, the precoding algorithms can be applied to the proposed channel matrix. Details can be found in the appended papers **B** and **C**.

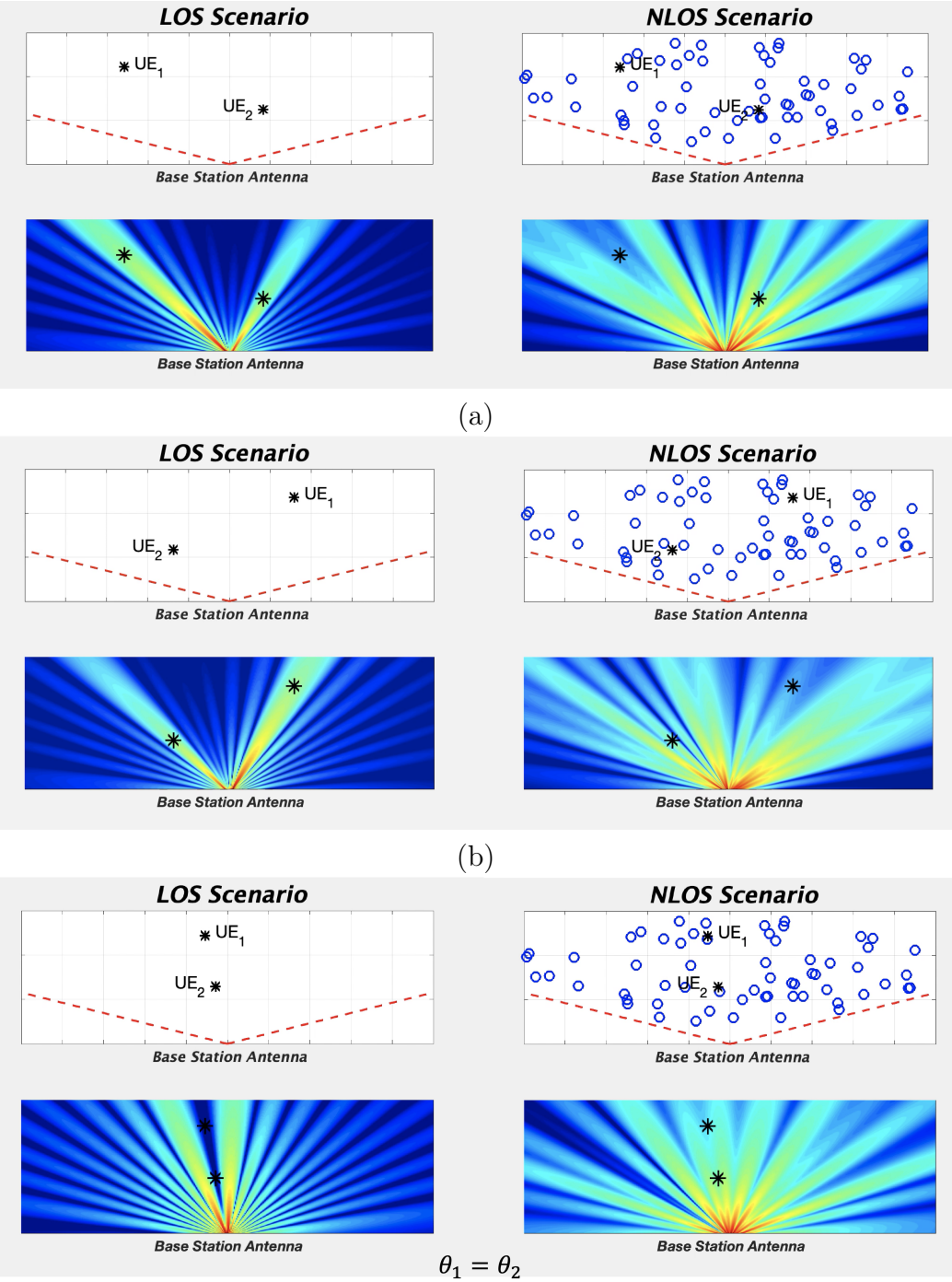

Figure 2.14: Radiation patterns of a linear base station antenna for different locations of two users in pure LOS and NLOS enviroments.

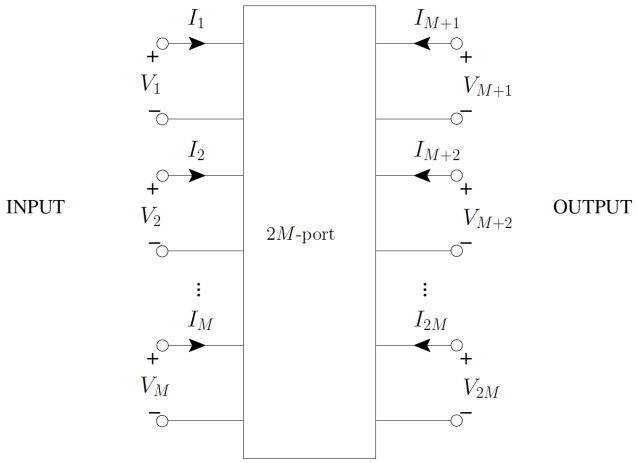

Figure 2.15: Multiport network model with M ports at the input and M ports at the output [21].

Chapter 3

Sparse Arrays: Pros and Cons

Half-wavelength inter-element spacing in antenna arrays is traditionally selected to avoid grating lobes or spatial aliasing. Sparse arrays can offer superior performance in comparison with regular arrays (uniform or periodic arrays with half a wavelength spacing). Although there exist different definitions for sparse arrays in the literature, in this work a sparse array is defined as an antenna array whose occupying aperture, given by the number of antenna elements, is larger than the conventional periodic array with 0.5λ spacing, where λ represents one wavelength. Therefore, a sparse array can be either periodic [35] or aperiodic [36].

Although better angular resolution can be achieved by the larger aperture of sparse arrays with a given number of antennas, their major drawback is the appearance of grating lobes [21, 37, 38]. This has been shown in the previous chapter in Fig. 2.7. This kind of drawback can be overcome in different ways depending on the application requirements. Following this, we will review the advantages of sparse arrays in various applications and discuss the way the grating lobe appearance is tackled. This review gives the reader insight into the synthesis of sparse arrays and possible solutions to overcome their drawbacks.

The potential advantages of sparse arrays have been already proven in several areas such as:

- Radio astronomy
- Satellite communication (SATCOM)
- Medical Imaging
- MIMO systems
- 5G base stations
- DOA estimation

The last two items are the focus of this thesis, so they are reviewed in the separate chapters 4 and 5.

3.1 Literature Review

3.1.1 Radio Astronomy

Interferometry is a technique in radio astronomy to capture high-resolution images of celestial objects [39]. Within this approach, instead of using a massive radio telescope, several smaller radio telescopes on earth are collecting the signal from an astronomical radio source. Correlating the signals at the output of each telescope produces the angular resolution of a much larger telescope whose aperture size is equal to the distance between the elements. Therefore, a spacing of hundreds of wavelengths or more is deployed between telescopes to get a narrow beamwidth and higher spatial resolution, though grating lobes emerge.

A square kilometre array interferometer (SKAI) requires an ultra wide-band frequency of operation. In order to achieve an efficient design, from a cost and complexity standpoint, ultra wide-band elements are commonly used for this purpose. Although the element spacing is around 0.5λ or even smaller at the lowest frequency, this value increases up to 5λ at the highest frequency [40]. Hence, grating lobes appear at higher frequencies of operation. In order to suppress the problem of grating lobes, the idea of random distribution of the elements in the antenna aperture successfully reduces the average SLL to e.g. -35 dB in [41].

Basically, the aforementioned technique disturbs the periodicity of the array, causing the grating lobes to be distributed over all angles. The main disadvantage of this approach is that individual element patterns differ from one another which makes the practical calibration more difficult. For instance, Fig. 3.1 from [42] compares the average EEP and the pattern of the central element of a periodic and aperiodic sparse array. Although the central element pattern resembles the average EEP in a regular array, these patterns differ significantly in an irregular array.

In order to suppress the problem of grating lobes in an interferometer, the stations can be rotated with respect to other stations and then their outputs are correlated [42], [43]. As an illustration, Fig. 3.2(a) and (b) show a two station configuration where the station B is rotated with respect to station A. As it is shown in Fig. 3.2(c) and (d), the main beam of the two stations remained unchanged while the grating lobes are rotated. Therefore, the multiplication of these two patterns results in suppressed grating lobes by the SLL of another station, shown in Fig. 3.2(e). The ultimate radiation pattern of eight rotated stations is depicted in Fig. 3.2(f). Grating lobes are converted to a set of increased side lobes, but they are still 20 dB below the main beam.

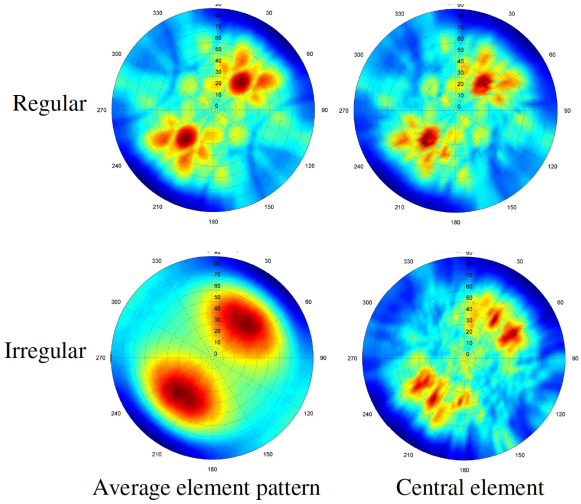

Figure 3.1: Average EEP (left column) compared with the embedded pattern of the central element (right column) of two array geometries: regular (top row) and irregular (bottom row) [42].

3.1.2 Satellite Communication (SATCOM)

In order to provide flexible coverage by satellite services, an active array with individually excited elements is an attractive alternative to conventional reflector antennas. Traditional periodic arrays suffer from the many hundreds of radiating elements and required radio-frequency (RF) chains, which increases the cost and weight significantly. Moreover, the required amplitude tapering across the array to satisfy a given pattern mask is not desirable from the PA point of view. This happens since the amplitude tapering requires the PAs to deliver different output power levels and therefore to work at different operating points, below the compression point, where the efficiency reduces. Hence, a sparse array with a reduced number of isophoric (equi-amplitude) radiators is highly desirable. However, synthesis of a sparse array due to its non-linearity and non-convexity is challenging. Publications regarding the synthesis of sparse arrays in the early sixties [45–49] show a great interest in the application of sparse arrays. A trade-off between the field-of-view (FOV) and possible grating (pseudo-grating) lobes of sparse arrays which adversely affect the SLL is discussed in [50]. Also therein, the synthesis of an isophoric sparse array generating steerable pencil beams for full earth coverage from GEO orbits is thoroughly explained. As it is shown in Fig. 3.3 the goal is to reduce the number of elements as much as possible while a specified pattern mask is satisfied.

An optimization algorithm which incorporates mutual coupling effects for the realization of a maximally sparse array is proposed in [51]. Moreover, paper [17] discusses the pros and cons of global optimization methods against analytical approaches to

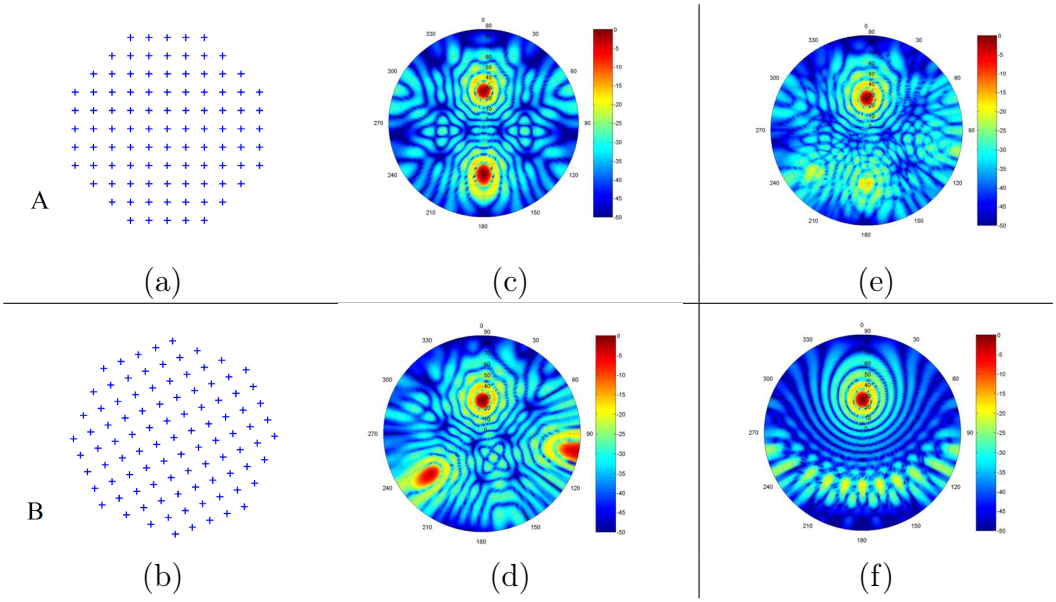

Figure 3.2: (a)-(b) Configuration of two sparse regular array stations ($d = 1.2\lambda$), (c)-(d) full-wave simulated radiation patterns of (a) and (b), respectively, (e) multiplied patterns of station A and B, (f) sumed pattern of eight cross correlated rotated stations [42].

synthesize a sparse array. It proposes a fast EM-compressive sensing based design method for large maximally sparse arrays, operating in a multibeam SATCOM scenario. In addition to the aforementioned references, a sparse array of widely spaced low power transmit-receive elements as a radio relay is proposed in [52]. Similar to this, the concept of a cluster of widely spaced satellites each accepting a small amount of transmit power is suggested in [53].

3.1.3 Medical Imaging

Sparse sampling has also been used for imaging purposes, especially in medical applications. An optimization framework to achieve a sparse array with optimized element weights and layout is proposed in [54] based on linear programming for ultrasound imaging. A genetic algorithm (GA), as a global optimizer, has been used in [55] for designing a sparse magnet array for portable magnetic resonance imaging (MRI). [56] argues that GA optimization is efficient for small two-dimensional (2D) arrays. It is stated that for 3D ultrasonic imaging, a large number of elements, about 16348, is required and simulated annealing (SA) [57] is a faster and more robust approach for large arrays. Fig. 3.4 illustrates a 2D array probe with its corresponding main and grating lobes. The optimization problem is tackled using SA by constraining the SLL while keeping the main beam width constant. Random sparsity (referred to as standard sparse array in [56]) and non-grid techniques are adapted. In the latter case,

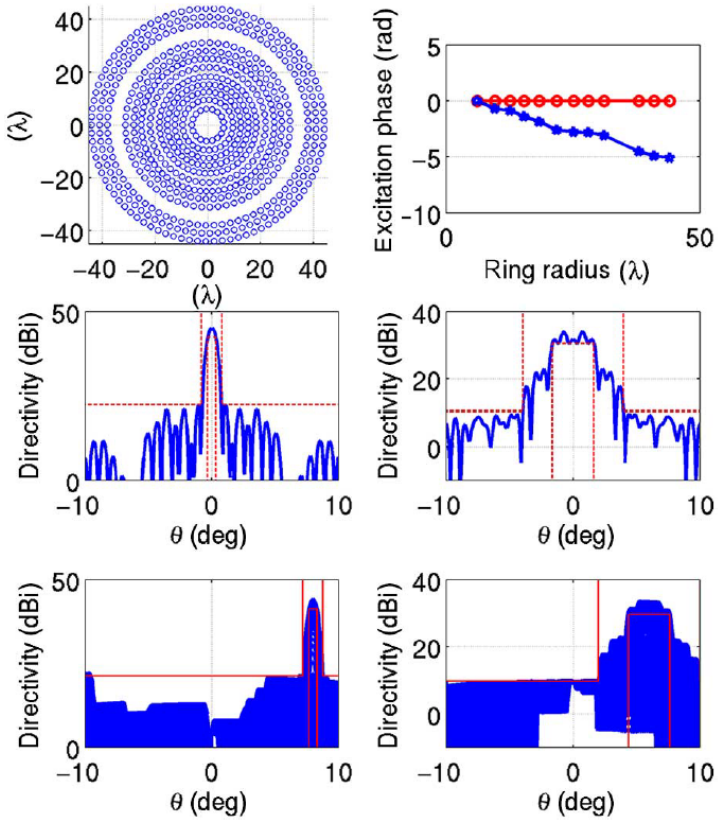

Figure 3.3: (first row) optimized array layout for both wide and narrow beams with corresponding phase excitations; (middle row) broadside patterns for both beams; (bottom row) scanned patterns for different ϕ-cuts [44].

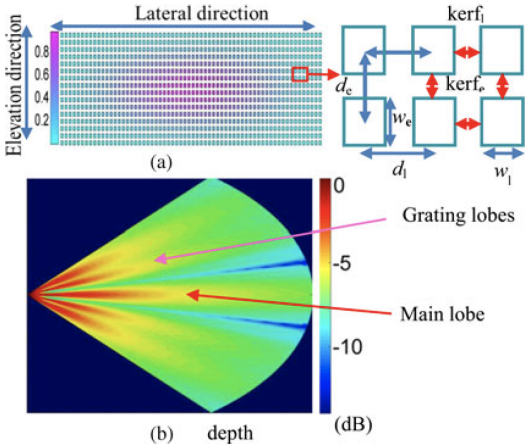

Figure 3.4: 2D probe array (a) excitation coefficients; (b) associated beam pattern [56].

the elements can be placed anywhere on the aperture surface. The suppression of the grating lobes in both planes is shown in Fig. 3.5. For further validation, simulated

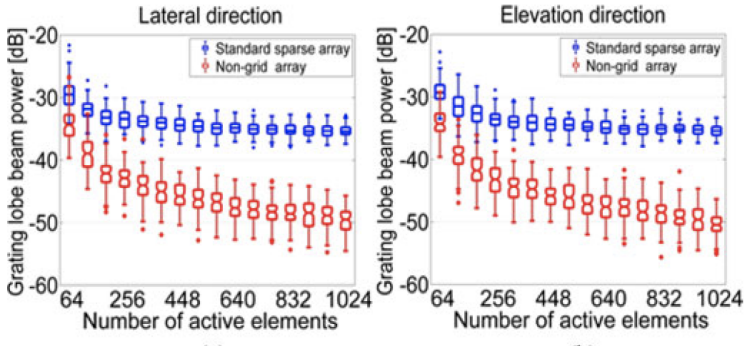

Figure 3.5: Grating lobe level in both horizontal and elevation planes as a function of active elements [56].

images of a tissue phantom with a biopsy needle using a $64 \times 16 = 1024$-element dense array, 177-element standard sparse array and 101-element optimized non-grid sparse array are presented in Fig. 3.6. All data are optimized to the peak echo achieved by the dense array. The energy loss by the sparse arrays due to the element reduction is about 18 dB with respect to the dense array. The echo from the needle is about 26 dB higher than the tissue using the dense array, while this value is about 25 dB for the two sparse arrays.

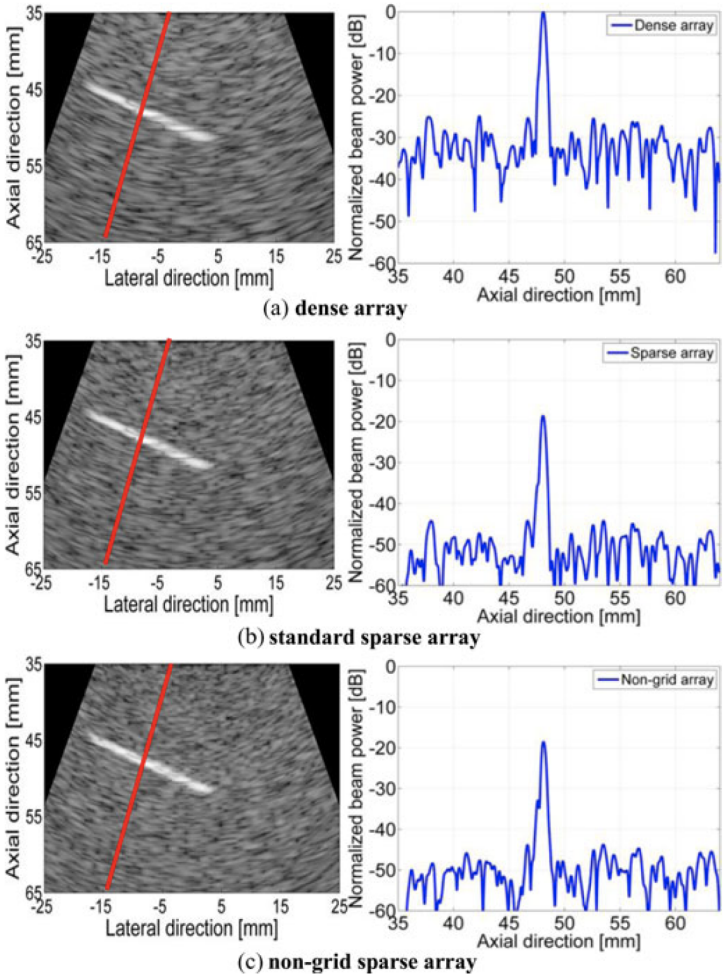

Figure 3.6: Imaging of a tissue phantom with a needle inside using (a) dense array with $64 \times 16 = 1024$ elements; (b) standard sparse array with 177 elements; (c) optimized non-grid sparse array with 101 elements [56].

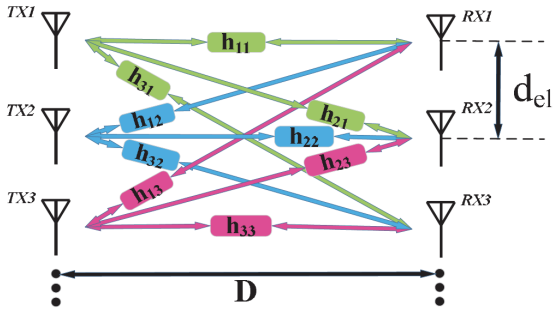

Figure 3.7: MIMO channel model with the same number of antennas at both TX and RX [58].

3.1.4 MIMO Systems

A MIMO system in a point-to-point fixed wireless access link is an efficient way of enhancing the channel capacity without demanding more spectrum. Therefore, it is a potential candidate for wireless backhaul networks, even at high frequencies. In a NLOS scenario, the eigenvalue decomposition technique is commonly applied to resolve orthogonal MIMO channels for spectral efficiency enhancement. However, in a LOS scenario the multipath components are weak and cannot contribute to an improvement of the channel capacity. Instead, artificial multipath, not caused by scatterers, can be created by increasing the element spacing to achieve spatial multiplexing.

Fig. 3.7, shows a schematic representation of a LOS MIMO channel for backhaul communication. In [59, 60], it is proven that there is an optimum inter-element spacing, depending on the frequency of operation, the link distance, and the number of antenna elements which maximizes the link capacity. Assuming D, M and N represent the link distance, the number of isotropic radiators at the transmitter (TX) and receiver (RX) sides, respectively, the optimum antenna separation is formulated as follows

$$d_t d_r = \frac{\lambda D}{\max(M, N)}, \tag{3.1}$$

where d_t and d_r denote the element spacing at the TX and RX, respectively, while $\max(M, N)$ selects the maximum value among M and N. For a 2×2 LOS MIMO system, the minimum optimal antenna separation (there could be several antenna separations which maximize the capacity) is plotted versus the link distance for different frequencies in Fig. 3.8 [59]. In general, decreasing the carrier frequency and increasing the link distance increases the optimal separation between the antenna elements. This example proves the potential advantage of sparse arrays for throughput enhancement.

Also, [58] and [61] propose reconfigurable MIMO antennas for different TX-RX separation distances. If the distance among TX-RX changes then a new optimal separation is required. Therefore, a mechanically or electronically reconfigurable antenna which results in an irregular MIMO configuration can restore the maximum channel capacity.

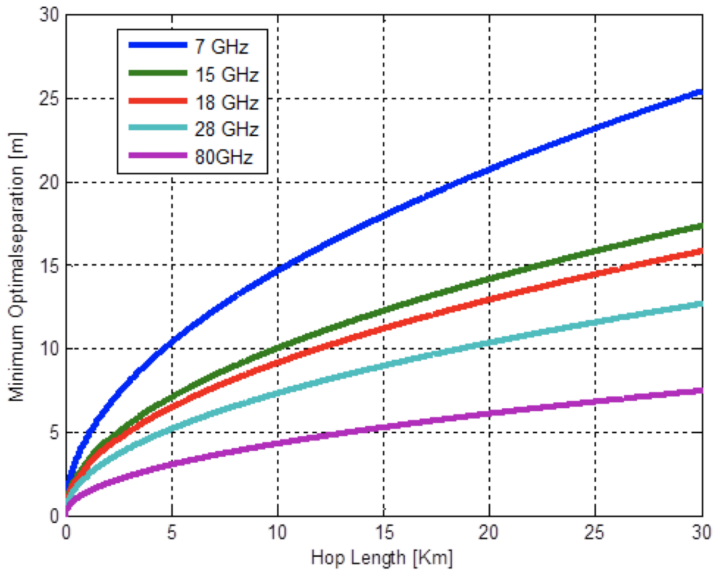

Figure 3.8: Minimum optimal antenna separation for a 2×2 LOS MIMO system at various carrier frequencies and link distances [59].

Chapter 4

Sparse Arrays for 5G Base Stations

4.1 MU-MIMO

A MU-MIMO system in which an antenna array serves multiple user equipments (UEs) over the same time-frequency resources is envisioned for the next generation of wireless communication. In [7], a hypothetically unlimited number of antennas at the base station is assumed; A base station with M antennas, where $M \to \infty$, serves K single-antenna users. Under this strong assumption, it is proved that the effects of fast fading, uncorrelated noise and intra-cell interference vanishes [7]. For illustration, consider a 2-UE case in an uplink scenario. The received signal at the base station is:

$$\mathbf{y} = \mathbf{h}_1 s_1 + \mathbf{h}_2 s_2 + \mathbf{n}, \tag{4.1}$$

where the channel vectors are assumed to be independent and identically distributed (i.i.d.) and their statistics follow $\mathcal{CN}(\mathbf{0}, \mathbf{I}_M)$. Considering maximum ratio combining (MRC) at the base station, the weight vector to distinguish the signal of UE_1, is the Hermitian of its corresponding channel vector, i.e.,

$$\mathbf{w}_1 = \frac{1}{M}\mathbf{h}_1^H. \tag{4.2}$$

To recover the signal of UE_1, multiplying (4.2) with (4.1):

$$\mathbf{w}_1\mathbf{y} = \frac{1}{M}\mathbf{h}_1^H\mathbf{h}_1 s_1 + \frac{1}{M}\mathbf{h}_1^H\mathbf{h}_2 s_2 + \frac{1}{M}\mathbf{h}_1^H\mathbf{n}. \tag{4.3}$$

When $M \to \infty$, based on the law of large numbers [62, 63]:

$$\begin{cases} \frac{1}{M}\mathbf{h}_1^H\mathbf{h}_1 = 1 \\ \frac{1}{M}\mathbf{h}_1^H\mathbf{h}_2 = 0 \\ \frac{1}{M}\mathbf{h}_1^H\mathbf{n} = 0 \end{cases} \tag{4.4}$$

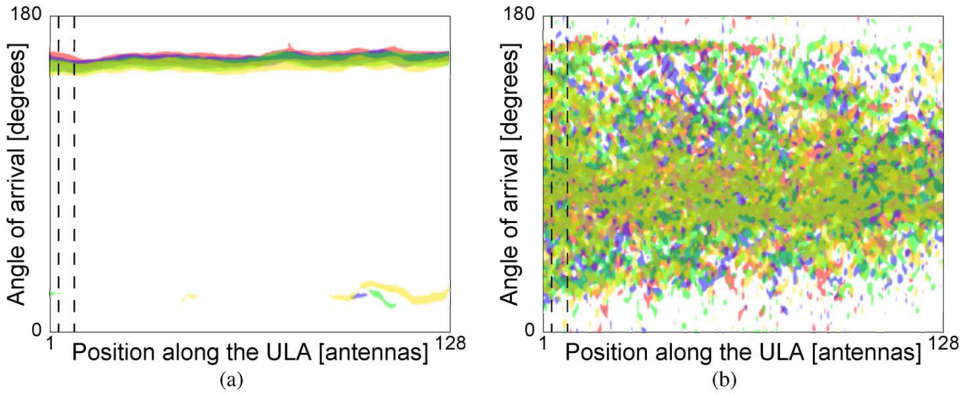

Figure 4.1: Spatial fingerprints in (a) a LOS scenario, (b) an NLOS scenario, where four users are co-located [64].

However, due to several practicalities, e.g., the routing of circuit components, integration in a compact size, thermal management, and complexity of signal processing algorithms, the number of antennas at the base station is limited. Therefore, the so-called favourable propagation [64] with orthogonal channel vectors seems unrealizable in realistic propagation environments, which means that UEs become spatially correlated.

4.1.1 Spatial Correlation

The spatial correlation between two UEs can be quantified by

$$\rho_{12} = \left| \frac{\mathbf{h}_1^H \mathbf{h}_2}{\|\mathbf{h}_1\| \, \|\mathbf{h}_2\|} \right|. \tag{4.5}$$

For the LOS scenario in Fig. 2.14(c), where $\theta_1 = \theta_2$, the correlation between two UEs is maximum, which is $\rho_{12} = 1$. Therefore, spatial correlation between close-by UEs in a LOS scenario is high and it is difficult to distinguish them in the spatial domain. However, as it was shown in the NLOS scenario in Fig. 2.14(c), the multipath scatterers help to decorrelate the UEs, to some extent. These effects are shown in [64], through a measurement campaign with a 128-element virtual ULA. As it is illustrated in Fig. 4.1, the angle of arrival from four co-located UEs in a LOS environment is almost the same. That is, high spatial correlation exists among them. However, for the same UEs' locations in the NLOS environment, the received signals from UEs are spread over angles. This large spatial variation decorrelates users, even when they are closely located in the angular domain.

It is evident that spatial correlation between channel vectors of UEs is a crucial metric, which indicates their distinguishability in the spatial domain. Sparse distribution of a given number of antennas at the base station can enhance the spatial

resolution. Hence, sparse arrays can play a critical role in SDMA systems. To illustrate the advantage of sparse arrays, we consider two close-by UEs with 2° angular difference in a LOS scenario. The base station is assumed to be a 16-element ULA with 0.5λ and 2λ spacings as regular and sparse arrays, respectively. ZF is applied at the base station to cancel the interference at UE_2.

Since ZF forces a null at the direction of interference (UE_2), the targeted UE (UE_1) does not receive the maximum by the regular array due to its wider beam pattern, as it is shown in Fig. 4.2(a). Meanwhile, a uniform sparse array is capable of nulling out the UE_2 when UE_1 receives the maximum signal. However, the appearance of grating lobes is obvious in Fig. 4.2(b). This may contribute to a high correlation between not necessarily close-by UEs. If the second UE is located around the direction of the grating lobe the correlation increases. Hence, the problem of grating lobes needs to be addressed properly.

4.2 Sparse Array Synthesis

Recent publications on the synthesis of sparse arrays for 5G base stations rely on optimization algorithms to satisfy certain pattern mask constraints. In [65], the problem is formulated as maximum SLL minimization for a given number of antennas with a pre-defined minimum inter-element spacing to avoid physically overlapping elements. The problem is convex and the CVX [66] platform is used. The initial array configuration is a periodic square grid array with 0.5λ spacing. Mutual coupling is neglected and hence similar element patterns are considered. The optimized array with its corresponding broadside and edge patterns are shown in Fig. 4.3.

In order to reduce the computational burden of the large array synthesis, a new iterative method called the "inflating-deflating exploration algorithm" is proposed [67]. The algorithm deploys a weighted l_1 minimization to maximally reduce the number of elements while desired pattern specifications are achieved. A planar grid of equispaced elements is used as a starting solution to initiate the algorithm. A maximum allowable inter-element spacing is determined to avoid grating lobes. Afterwards, convex optimization is used to find a sparse layout. The synthesized sparse linear array with element locations and their corresponding excitation amplitudes are shown in Fig. 4.4(a). The radiation pattern is shown in Fig. 4.4(b). The algorithm is used in [68] for 5G applications and beyond.

A co-design technique aiming at synthesizing both the array layout and radiating element geometry to achieve a pre-defined side lobe mask for all scan angles and operating frequencies is presented in [69]. The proposed approach is claimed to significantly mitigate the complexity of the feed network by irregular and joint clustering of the excitation magnitudes and phases. GA is adapted for determining clustered sub-arrays.

All the above-mentioned references try to synthesize an unconventional array for

5G base station based on a pre-defined pattern mask. However, as it was explained for the NLOS scenario in Fig. 2.14(c), due to the multipath propagation, classical antenna metrics are indirect figure-of-merits for a wireless communication link. In fact, a MU-MIMO system in a realistic environment should be able to spatially distribute the available power into the wireless channel in a way that multipath components are added at the location of a UE, regardless of directivity, HPBW and SLL of the base station. Therefore, a new synthesis method considering the end-performance of a communication link as a cost function is necessitated.

Recently, a capacity-driven array synthesis which aims at maximizing the overall system capacity is proposed in [70]. The paper takes two approaches for excitation-only synthesis, i.e., directivity maximization as the traditional approach and capacity maximization as a novel approach, to illustrate the non-negligible performance difference. Radiation patterns of synthesized arrays, for different scenarios, are plotted in Fig. 4.5. In the left column of Fig. 4.5 the array is synthesized for capacity maximization while in the right column directivity maximization is applied. Therefore, a clear main beam and controlled SLL are observed in the right column, while in the left column the radiated power is spatially spread over a wide range of angles. The base station serves 16 randomly located UEs. The capacity and SLL plots versus the l-th UE is shown in Fig. 4.6. As can be observed in Fig. 4.6(a), the directivity maximization approach provides lower SLL for two different polarizations, in comparison with the capacity maximization technique. However, the latter approach leads to higher capacity per UE, as depicted in Fig. 4.6(b).

A novel hybrid optimization approach to enhance the average capacity in a MU-MIMO system, by improving the GA performance through a reliable initial guess, is proposed in the appended paper **E**.

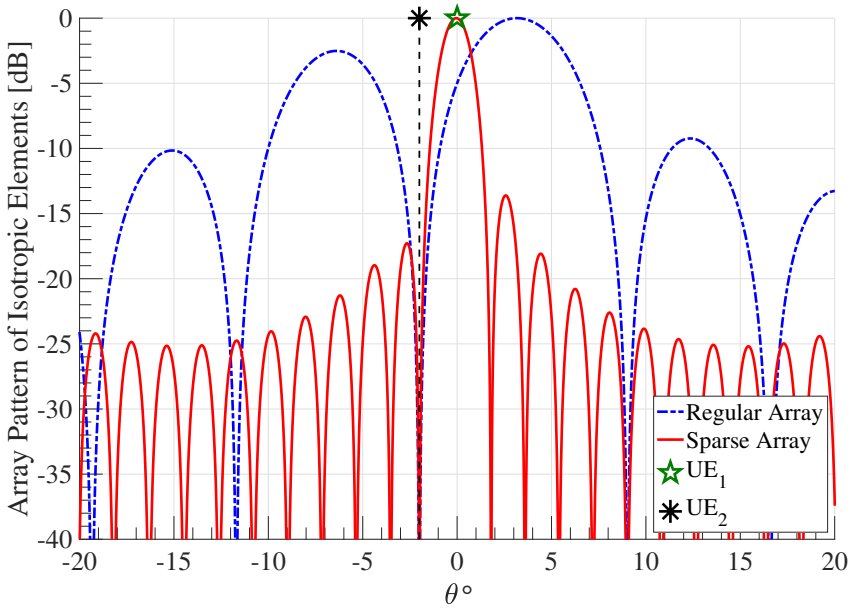

(a)

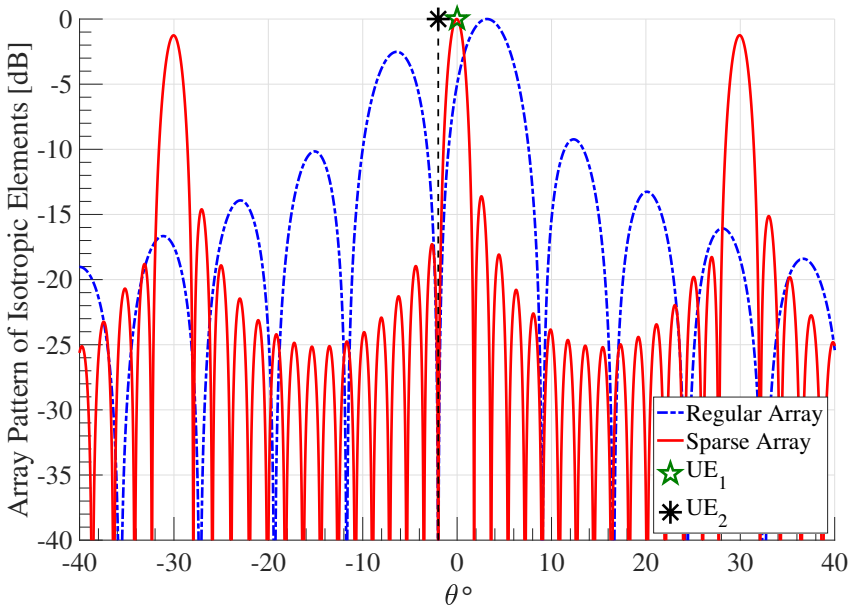

(b)

Figure 4.2: Radiation patterns of regular and sparse linear base station antenna arrays applying ZF precoder to serve UE_1.

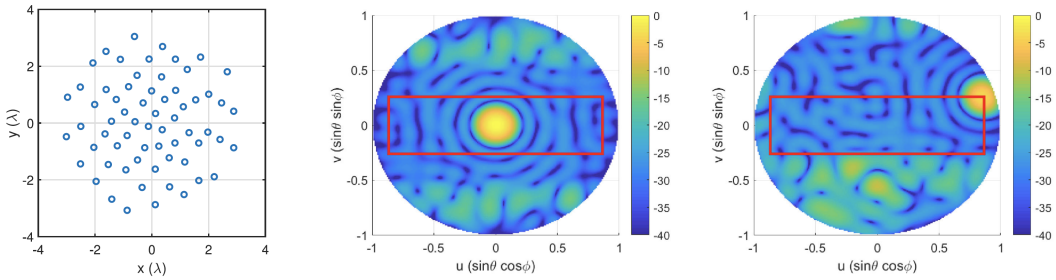

(a) (b)

Figure 4.3: Optimized layout of the sparse array with its corresponding broadside and corner radiation patterns presented in [65].

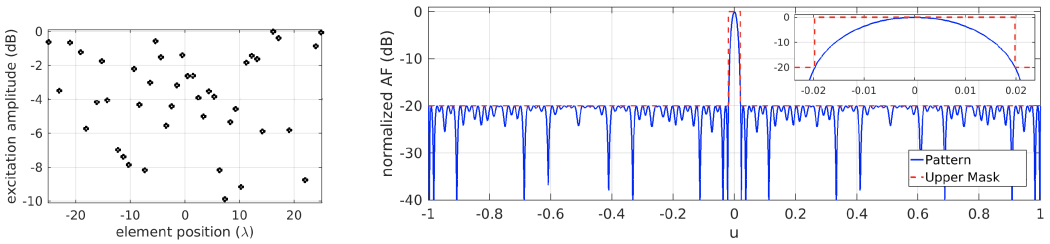

(a) (b)

Figure 4.4: Optimized layout of the sparse array with its corresponding radiation pattern satisfying the pre-defined pattern mask, presented in [67].

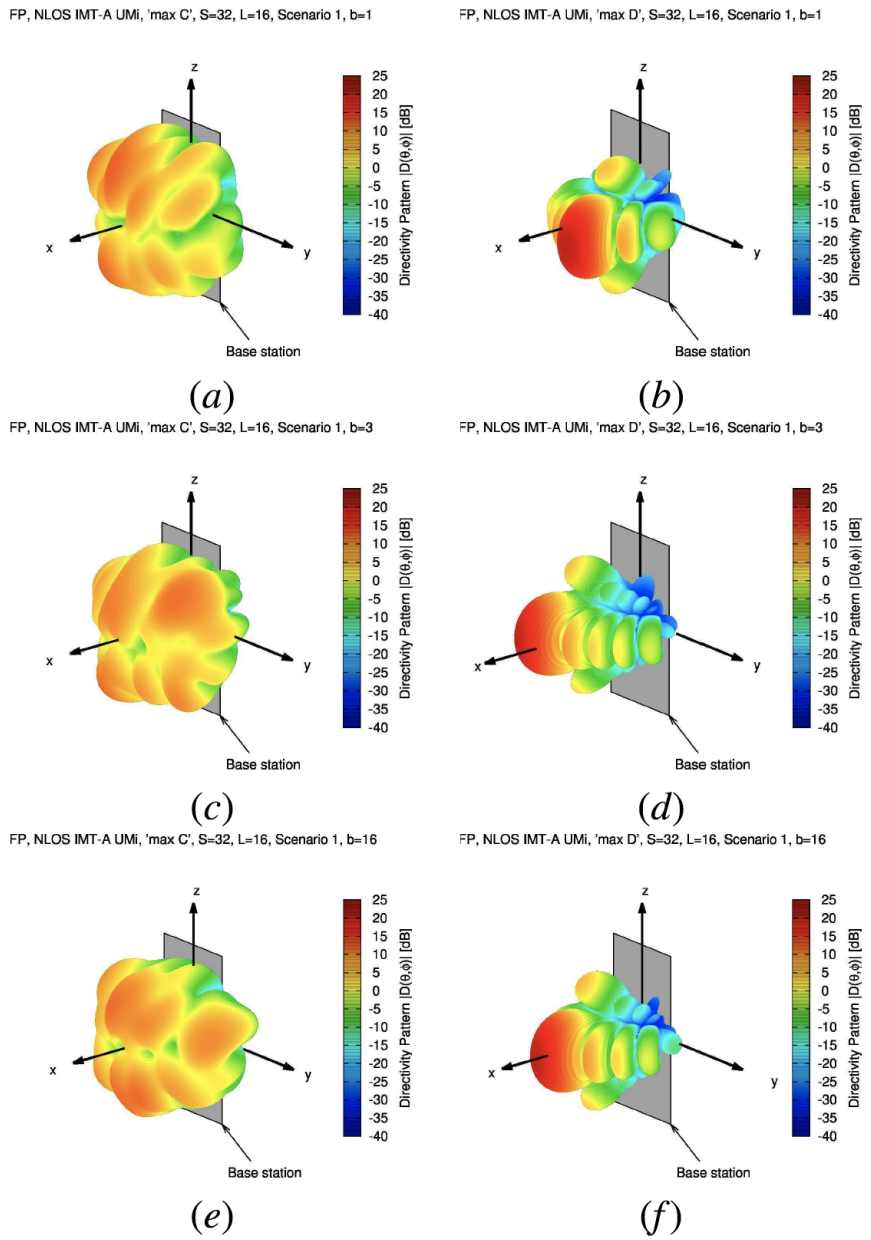

Figure 4.5: Radiation patterns of a fully populated planar array with excitation synthesis achieved by (a), (c) and (e) capacity maximization approach; (b), (d) and (f) directivity maximization approach [70].

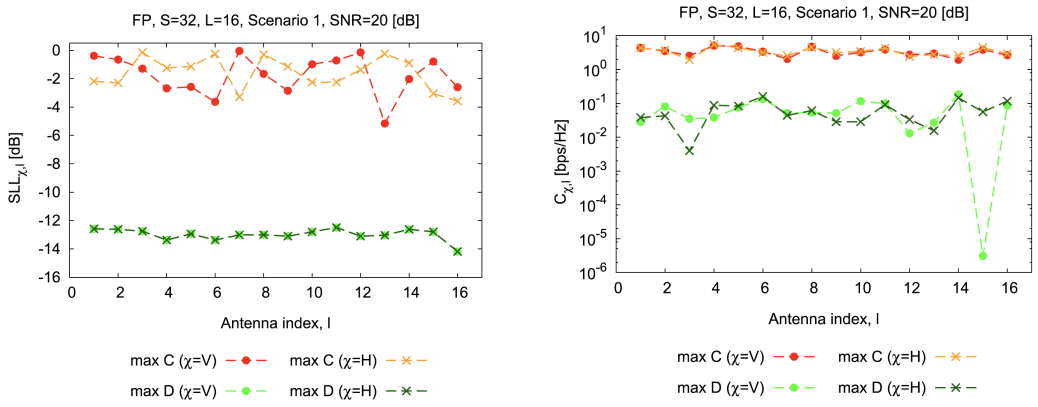

(a) (b)

Figure 4.6: SLL and capacity plots versus the l-th UE index for two polarizations achieved by directivity and capacity maximization approaches [70].

Chapter 5

Sparse Arrays for Direction-of-Arrival (DOA) Estimation

5.1 DOA Estimation

Direction finding using antenna arrays has been traditionally investigated for localization and tracking purposes [71]. The topic is vastly studied in the signal processing community, where traditional algorithms are well-developed for uniform arrays [72]. Subspace based methods, e.g., MUSIC [73], are proposed for applications which require high resolution. Recently, new array configurations, i.e., non-uniform sparse arrays, are deployed to enhance the radar angular resolution. In this chapter, we review the fundamentals of DOA estimation. Furthermore, different sparse array configurations which are proposed to enhance the DOA estimation accuracy are discussed.

5.1.1 Received Signal Model

Assume K uncorrelated narrowband far-field sources that transmit a signal to a ULA. The received signal vector is the superposition of signals from all sources and can be represented by [74]:

$$\mathbf{x}(t) = \sum_{k=1}^{K} \mathbf{a}(\theta_k) s_k(t) + \mathbf{n}(t), \tag{5.1}$$

where $s_k(t)$ is the incoming plane wave transmitted by the k-th source at time t from the direction θ_k and $\mathbf{n}(t)$ is the additive noise. $\mathbf{a}(\theta_k)$ is the array steering vector,

which for an L-element ULA can be represented by

$$\mathbf{a}(\theta_k) = \begin{bmatrix} 1 \\ e^{j\frac{2\pi}{\lambda}d\sin\theta_k} \\ e^{j\frac{2\pi}{\lambda}2d\sin\theta_k} \\ \vdots \\ e^{j\frac{2\pi}{\lambda}(L-1)d\sin\theta_k} \end{bmatrix}. \tag{5.2}$$

A single observation of the received signal vector $\mathbf{x}(t)$ is known as a snapshot.

A matrix representation of (5.1) is

$$\mathbf{x}(t) = \mathbf{A}\mathbf{s}(t) + \mathbf{n}(t), \tag{5.3}$$

where $\mathbf{A} \in \mathbb{C}^{L\times K}$ is the array manifold and $\mathbf{s}(t) \in \mathbb{C}^{K\times 1}$ is a vector of incoming signals, i.e.,

$$\mathbf{A} = [\mathbf{a}(\theta_1), \mathbf{a}(\theta_2), \ldots, \mathbf{a}(\theta_k)] \tag{5.4}$$

$$\mathbf{s}(t) = [s_1(t), s_2(t), \ldots, s_K(t)]^T \tag{5.5}$$

The received and desired signal autocovariance matrices are defined by:

$$\mathbf{R}_{xx} = \mathbb{E}\{\mathbf{x}(t)\mathbf{x}^H(t)\}, \tag{5.6}$$

$$\mathbf{R}_{ss} = \mathbb{E}\{\mathbf{s}(t)\mathbf{s}^H(t)\}, \tag{5.7}$$

where the expectation operator is denoted by $\mathbb{E}$. In practice, the expected value is approximated by sufficiently enough number of snapshots (N)

$$\mathbf{R}_{xx} = \frac{1}{N}\sum_{n=1}^{N}\mathbf{x}(t)\mathbf{x}^H(t). \tag{5.8}$$

The conventional beamforming method scans across the angular region of interest and whichever direction maximizes the output power is the estimate of the desired signal direction. The output power of the beamformer, referred to as the spatial spectrum, is formulated as [72, 74]

$$P(\theta) = \frac{\mathbf{a}^H(\theta)\mathbf{R}_{xx}\mathbf{a}(\theta)}{\mathbf{a}^H(\theta)\mathbf{a}(\theta)}. \tag{5.9}$$

5.1.2 MUSIC Algorithm

Subspace based methods are the other main class of DOA estimation algorithms, resulting in high spatial resolution. The received signal space can be separated in two parts: signal subspace and noise subspace. The subspace spanned by the columns

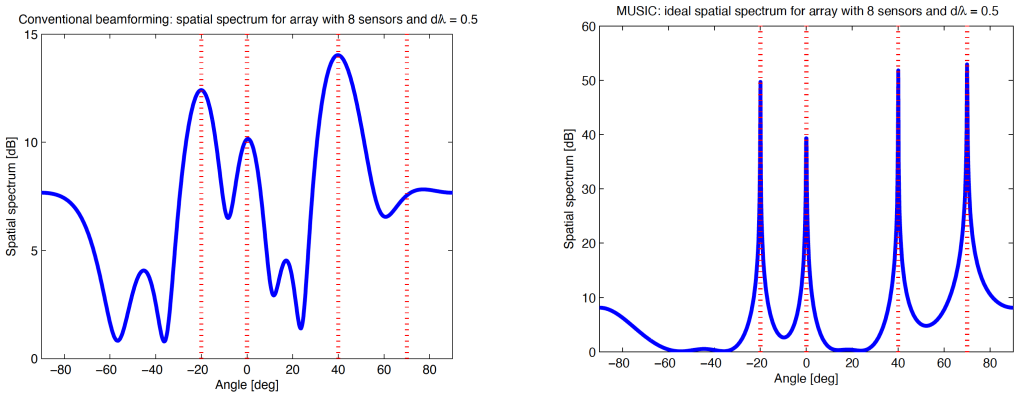

(a) (b)

Figure 5.1: DOA estimation of four sources located at $[-20°, 0°, 40°, 70°]$ using conventional and MUSIC algorithms [75].

of $\mathbf{A}$ is denoted as signal subspace and the subspace orthogonal to the signal subspace is known as noise subspace. The subspace algorithm exploits this orthogonality for the DOA estimation. The MUSIC algorithm employs the eigenvalue decomposition (EVD). It can be summarized as [73]:

- compute/estimate $\mathbf{R}_{xx}$
- compute EVD of $\mathbf{R}_{xx}$ and split signal-noise subspace
- compute projection matrix: $\mathbf{P}_n = \mathbf{U}_n\mathbf{U}_n^H$, where $\mathbf{U}_n$ is the unitary matrix of the noise subspace.
- evaluate the pseudo spectrum

$$P_{\text{MUSIC}}(\theta) = \frac{\mathbf{a}^H(\theta)\mathbf{a}(\theta)}{\mathbf{a}^H(\theta)\mathbf{U}_n\mathbf{U}_n^H\mathbf{a}(\theta)}. \tag{5.10}$$

The number of sources which can be detected by an L-element ULA, using MUSIC, is $L-1$. As an illustration, the spatial spectra of an 8-element array for DOA estimation of four sources located at $[-20°, 0°, 40°, 70°]$ using conventional and MUSIC algorithms are compared in Fig. 5.1. As can be observed, better angular resolution is achieved by the MUSIC algorithm.

5.1.3 Spatial Smoothing

In automotive radars, DOA estimation plays a critical role in distinguishing sources in one range-velocity bin. However, due to the high speed of vehicles and highly dynamic environments, there is no time to collect several snapshots for estimating

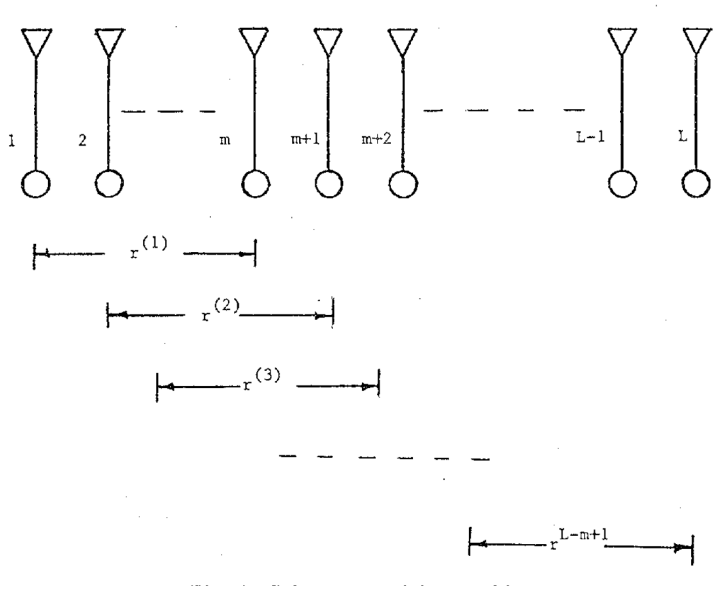

Figure 5.2: Subarray spatial smoothing [19].

the received signal covariance matrix as explained in equation (5.8). In the limit, the DOA estimation needs to be accomplished using a single snapshot. In this case, the sources are fully correlated, known as coherent sources, which results in DOA estimation failure. A solution is proposed for a ULA, by dividing it into similar overlapping subarrays of size m, as it is shown in Fig. 5.2. The covariance matrix of the p-th subarray is denoted by $\mathbf{R}_p$. Afterwards, the spatially smoothed covariance matrix is determined as the sample mean of covariance matrices of the overlapping sub-arrays:

$$\mathbf{R} = \frac{1}{M} \sum_{p=1}^{M} \mathbf{R}_p, \tag{5.11}$$

where $M = L - m + 1$ is the number of subarrays.

5.1.4 Co-prime Arrays

With a given number of elements, sparse arrays are proposed to dramatically increase the degrees-of-freedom (DOF) in the DOA estimation problem. This results in resolving more sources than the number of physical sensors which equivalently increases the spatial resolution of the radar [16].

By deploying orthogonal waveforms at the transmitter elements, MIMO radars have successfully achieved superior performance in comparison with phased array radars by the realization of an extended virtual array with increased DOF [76]. The maximum achievable DOF using a MIMO radar, assuming M-element TX and N-element RX antennas, is MN depending on the array topologies. Minimum re-

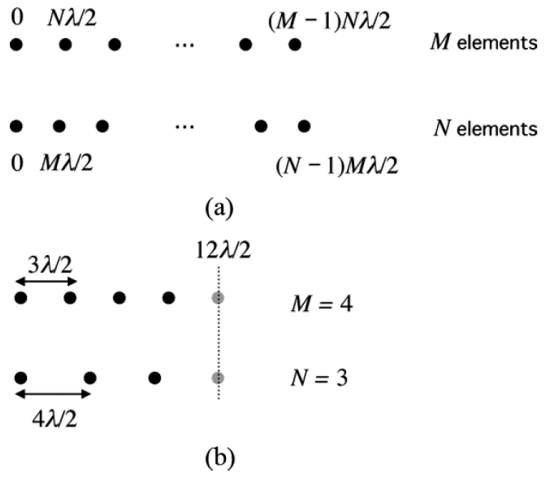

Figure 5.3: (a) ULA with co-prime array configuration, (b) an example where $M = 4$ and $N = 3$ [16].

dundancy arrays (MRA) [15] are known as a class of linear arrays with a maximal resolution by an intelligent placement of elements which minimizes the number of redundant spacings. Other types of sparse arrays which have been proposed to be used in a DOA estimation problem for DOF enhancement can be listed as co-prime arrays [16], nested arrays [77] and sparse ruler arrays [78]. As an example, Fig. 5.3 shows the configuration of a co-prime array, comprised of two sets of ULAs. One ULA with M sensors has an inter-element spacing of $N\lambda/2$ and the second ULA consists of N sensors with $M\lambda/2$ spacing. The required design criterion is that M and N are co-prime. Upon a beampattern multiplication of these two ULAs, due to the co-primality, the grating lobes of the first ULA is suppressed by the low radiation of the second ULA and vice versa.

5.1.5 Nested Arrays

Another type of sparse array proposed for enhanced DOA estimation is nested arrays [77]. It is the concatenation of two ULAs, called inner and outer arrays. The inner ULA comprises of N_1 elements with d_1 spacing and the outer ULA has N_2 elements with d_2 spacing. The element spacing in the outer array follows $d_2 = (N_1+1)d_1$, as it is shown in Fig. 5.4. The array configuration is similar to the MIMO radar. However, the major difference is that the nested array is used for receive only (passive sensing) instead of active sensing. The working principle is based on the generation of a difference co-array, which is a filled ULA with $2N_2(N_1 + 1) - 1$ elements. An example of DOA estimation using co-prime and nested arrays for detection of more sources than the number of physical sensors is shown in Fig. 5.5.

It is to be noted that the generation of difference co-array from co-prime and

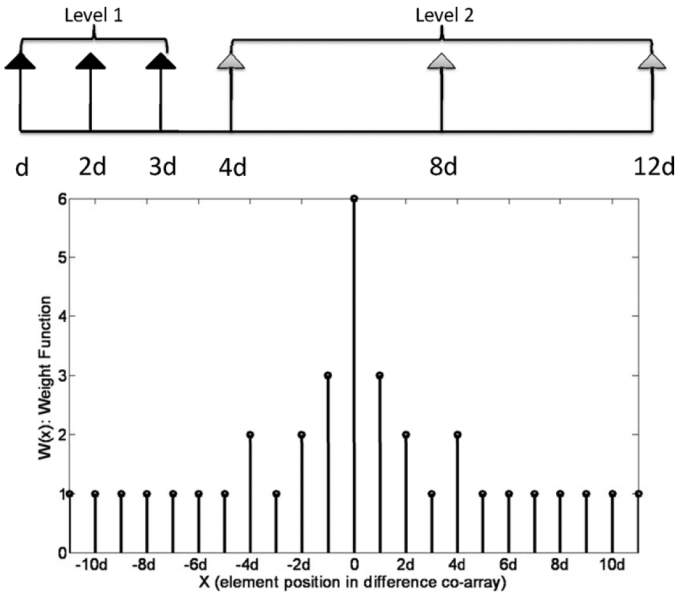

Figure 5.4: A 2-level nested array with 3 lemenets in each level and its corresponding difference co-array with 23 elements [77].

nested arrays is based on the vectorization of the received signal covariance matrix. It is only valid with the assumption of temporally uncorrelated sources [77, 79]. This is obviously not the case in an automotive application where the number of snapshots is limited and therefore the covariance matrix becomes rank deficient. Sparse signal recovery algorithms are proposed for single snapshot DOA estimation [80], however, they suffer from an increased computational burden [81, 82]. Therefore, high-resolution single snapshot DOA estimation using sparse arrays compatible with low complexity algorithms is highly desirable for the automotive industry. A novel solution can be found in the appended paper **F**.

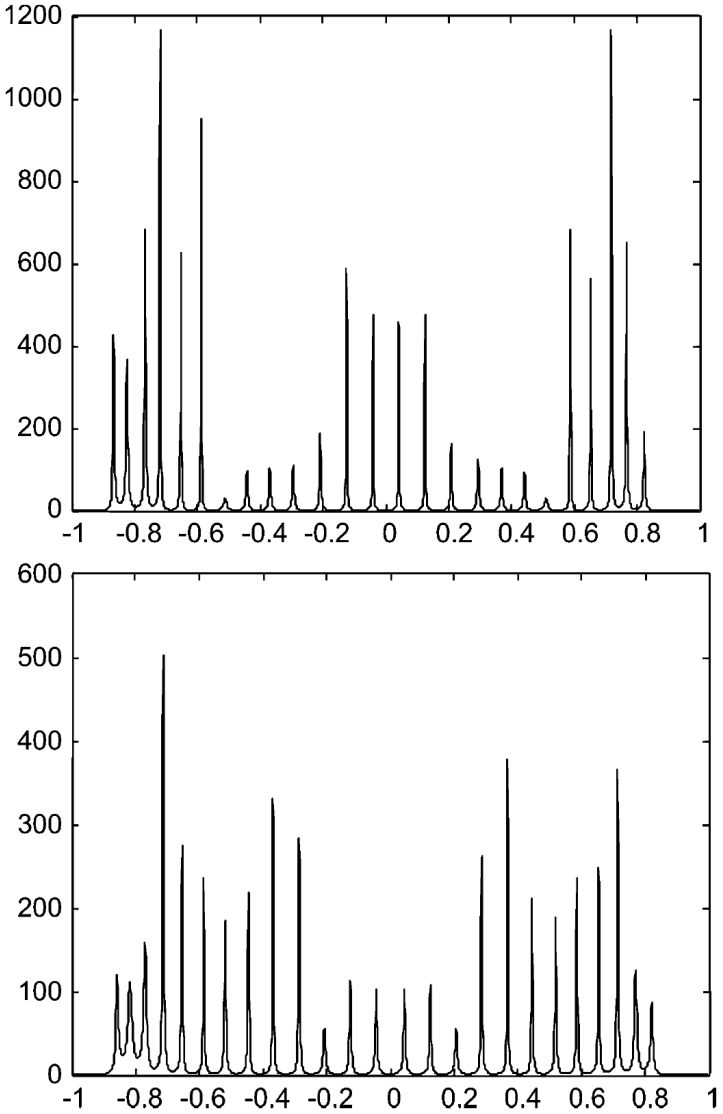

Figure 5.5: DOA estimation of 25 sources using co-prime sampling (top, $M = 7$, $N = 11$) and nested sampling (bottom, $N_1 = 7$, $N_2 = 11$). SNR = 30 dB and 300 snapshots were used [16].

Chapter 6

Contributions and Future Work

6.1 Contributions

In the previous introductory chapters, we have reviewed the fundamentals of antenna arrays, MIMO antennas, a beamforming concept in MU-MIMO scenarios, applicable network theory, and DOA estimation. Potential advantages of sparse arrays and solutions to suppress their corresponding drawbacks for 5G base station and radar applications have been discussed. It has been shown that a sparse distribution of a given number of antenna elements can facilitate implementation complexities of mm-wave 5G antennas. Meanwhile, it improves the angular resolution which is highly desirable in SDMA systems. Sparsity has also been observed useful for high-resolution DOA estimation. In this chapter, we present a summary of the appended papers in part II. In addition, possible future work directions are briefly discussed.

Paper A: Per-Antenna Power Distribution of a Zero-Forcing Beamformed ULA in pure LOS MU-MIMO

This paper proposes an analytical model to determine the per-antenna power distribution of an M-element ULA as a BSA when ZF is applied as a downlink precoder. While many papers consider a total transmit power constraint in their analysis, this paper suggests that there should be a limit on the per-antenna power since it may vary a lot from one antenna to another, depending on the correlation between the channel vectors. In order to maintain the analytical tractability of the analysis, we assume only two UEs in the FOV of the BSA, however, the general conclusions, specifically for the case of highly correlated channel vectors, remain valid for the multi-user case. The analytical investigation proves that the power distribution across the BSA is a periodic function depending on the angular

separation between two UEs, the inter-element spacing and the wavelength. Also, it is shown that increasing the inter-element spacing reduces the periodicity of the power distribution function and consequently less power variation across the ULA can be observed. In order to prevent grating lobes to appear inside the visible region by a periodic sparse array, an upper bound depending on the FOV is given for the inter-element spacing.

Paper B: Network Model of a 5G MIMO Base Station Antenna in a Downlink Multi-User Scenario

In this paper, we propose a system-level network model of a 5G BSA in a downlink MU-MIMO system as a link budget analyzer. The intriguing property of this network model is that it incorporates antenna effects into the channel matrix. While the common approach in the Wireless Community is to normalize the weight matrix for the power allocation, we avoid it in this paper to compute the actual per-antenna power for satisfying a required data rate in the link. To this end, the transmitter and receiver port voltages/currents are related through impedance sub-matrices. Based on the new $(K + M)$-port network model, the $K \times M$ channel matrix which includes antenna mutual coupling, EEPs, and polarimetric effects is extracted. Upon applying the ZF beamformer, the required EIRP with and without mutual coupling effects are computed and compared.

Paper C: Multi-Panel Sparse Base Station Design with Physical Antenna Effects in Massive MU-MIMO

Based on the network model in Paper B, a co-simulation platform is presented for a 5G BSA design. This paper also proposes a sectorized BSA with limited FOV per sector and deploys directive antenna elements for grating lobe suppression. One antenna panel, which covers a wide FOV of 120 degrees and comprises many elements, is replaced by L tilted panels employing L times fewer elements and L times smaller FOV per panel. While a LOS scenario is discussed in the previous paper, we propose a generic approach to model multipath effects in the network model namely by employing randomly localized clusters of scatterers (COSs). While close-by UEs result in highly correlated channel vectors in a LOS scenario, it is shown that the multipath effect can decorrelate the UEs, to some extent, in a NLOS environment. The mismatch effect at the antenna input ports due to the beamforming is quantified by the decoupling efficiency through the active impedances. Sparsity in multiple panels is seen useful for mismatch reduction when beamforming is applied. Finally, the proposed multi-panel sparse configuration is demonstrating a superior sum-rate performance with respect to a single panel ULA

in different propagation environments.

Paper D: Array Configuration Effect on the Spatial Correlation of MU-MIMO Channels in NLoS Environments

In this paper, an electromagnetic model of a NLOS channel is proposed where scatterers are considered as resonant dipoles in CoSs. The scattered field from resonant dipoles is computed analytically and validated through full-wave numerical simulations. Afterwards, sparsity and aperiodicity at the base station are examined in terms of inter-user spatial correlation in a 2D NLOS environment. It is shown that the sparsity (increased inter-element spacing) decreases the probability of high correlation between two UEs in a NLOS scenario. Further improvement is observed by an aperiodic distribution of a given number of antennas into the sparse antenna aperture.

Paper E: Sparse Array Synthesis Including Mutual Coupling for MU-MIMO Average Capacity Maximization

Array synthesis in the EM community commonly uses an optimization algorithm to synthesize the array radiation pattern while mutual coupling is assumed negligible. The main novelty of this work is to propose a capacity-driven array synthesis in the presence of mutual coupling for a MU-MIMO system. We show that the appearance of grating lobes is degrading for the system capacity and cannot be disregarded in a MU communication where SDMA is applied. With the aid of array sparsity and aperiodicity, the adverse effects of grating lobes and mutual coupling are suppressed and capacity is enhanced. This is performed by proposing a two-phase optimization strategy. In Phase I, the problem is relaxed to a convex optimization problem by ignoring the mutual coupling and weakening the constraints. The solution of Phase I is used as the initial guess for the GA in phase II, where the mutual coupling is taken into account. The proposed hybrid algorithm outperforms the conventional GA with random initialization.

Paper F: Sparse Automotive MIMO Radar for Super-Resolution Single Snapshot DoA Estimation with Mutual Coupling

A novel sparse MIMO radar is presented for high-resolution single snapshot DOA estimation in the presence of mutual coupling. Both the transmitter and receiver arrays are divided into uniform sparse sub-arrays with different inter-element spacings. Therefore, two uniform sparse virtual arrays are realizable based on the MIMO radar concept. Due to the uniformity of virtual arrays, the spatial smoothing algorithm can be applied for the suppression of temporal correlation

among sources. Afterwards, the co-primality of spatially smoothed virtual arrays avoids spatial aliasing. The received signal model incorporates physical antenna effects via open-circuited EEPs and a coupling matrix based on the impedance parameters. It is observed that the mutual coupling can cause DOA estimation error.

6.2 Future Work

In one of the 3rd Generation Partnership Project (3GPP) meetings, it is argued that a multi-panel configuration is very likely to be used as a 5G new radio (NR) implementation especially for high frequency bands [83]. Hence, the multi-panel antenna structure may well be developed to cope with the practicalities and implementation issues of a massive MIMO system. We took additional steps and proposed tilted panels of sparse arrays, however, the applicability of the new structure and the grating lobe mitigation need to be assessed in practice.

A two-phase optimization algorithm is deployed to design a linear irregular sparse array which maximizes the average capacity in a MU-MIMO system. The algorithm can be expanded to planar arrays with 3D beamforming capability. The performance of uniform and irregular planar arrays can be compared in terms of average capacity. In addition, the algorithm is well developed for minimum scattering antennas. It is worthwhile to examine the irregular array distribution, as the outcome of the optimization algorithm, with realistic antenna elements, e.g., patch antennas, to see whether the same performance improvement can be achieved.

The performance of the novel MIMO radar in terms of high-resolution DOA estimation needs to be validated through measurements. Also, automotive radar is responsible for several estimation tasks, e.g., range, velocity, height and angle. The functionality of the proposed sparse MIMO radar for parameter estimation other than DOA estimation needs to be scrutinized.

References

[1] −, "Cisco visual networking index: Forecast and trends, 2017-2022," [Online] Available: *https://www.cisco.com/c/en/us/solutions/collateral/service-provider/visual-networking-index-vni/white-paper-c11-741490.html*, Nov. 2018.

[2] X. Wang, L. Kong, F. Kong, F. Qiu, M. Xia, S. Arnon, and G. Chen, "Millimeter wave communication: A comprehensive survey," *IEEE Commun. Surveys Tuts.*, vol. 20, no. 3, pp. 1616–1653, 2018.

[3] I. A. Hemadeh, K. Satyanarayana, M. El-Hajjar, and L. Hanzo, "Millimeter-wave communications: Physical channel models, design considerations, antenna constructions, and link-budget," *IEEE Commun. Surveys Tuts.*, vol. 20, no. 2, pp. 870–913, 2017.

[4] S. M. Patole, M. Torlak, D. Wang, and M. Ali, "Automotive radars a review of signal processing techniques," *IEEE Signal Process. Mag.*, vol. 34, no. 2, pp. 22–35, Mar. 2017.

[5] I. WP5D, "Technical feasibility of IMT in bands above 6 GHz," 2015.

[6] T. S. Rappaport, G. R. MacCartney, S. Sun, H. Yan, and S. Deng, "Small-scale, local area, and transitional millimeter wave propagation for 5G communications," *IEEE Trans. Antennas Propag.*, vol. 65, no. 12, pp. 6474–6490, Dec. 2017.

[7] T. L. Marzetta, "Noncooperative cellular wireless with unlimited numbers of base station antennas," *IEEE Trans. Wireless Commun.*, vol. 9, no. 11, pp. 3590–3600, Nov. 2010.

[8] C. Farsakh and J. A. Nossek, "Application of space division multiple access to mobile radio," in *Proc. Int. Symp. Personal, Indoor Mobile Radio Commun.* The Hague, The Netherlands, 1994, pp. 736–739.

[9] Y. Huang, Y. Li, H. Ren, J. Lu, and W. Zhang, "Multi-panel MIMO in 5G," *IEEE Commun. Mag.*, vol. 56, no. 3, pp. 56–61, Mar. 2018.

[10] B. Döring, "Cooling system for a Ka band transmit antenna array," *Internal Report, DLR-IB 554–06/02*, 2005.

[11] C. M. Chen, V. Volski, L. Van der Perre, G. A. Vandenbosch, and S. Pollin, "Finite large antenna arrays for massive MIMO: characterization and system impact," *IEEE Trans. Antennas Propag.*, vol. 65, no. 12, pp. 6712–6720, Dec. 2017.

[12] J. Hasch, E. Topak, R. Schnabel, T. Zwick, R. Weigel, and C. Waldschmidt, "Millimeter-wave technology for automotive radar sensors in the 77 GHz frequency band," *IEEE Trans. Microw. Theory Techn.*, vol. 60, no. 3, pp. 845–860, Mar. 2012.

[13] E. Fishler, A. Haimovich, R. Blum, D. Chizhik, L. Cimini, and R. Valenzuela, "MIMO radar: An idea whose time has come," in *Proc. IEEE Radar Conf.*, 2004, pp. 71–78.

[14] F. C. Robey, S. Coutts, D. Weikle, J. C. McHarg, and K. Cuomo, "MIMO radar theory and experimental results," in *Proc. 38th Asilomar Conf. Signals, Syst. Comput.*, vol. 1, 2004, pp. 300–304.

[15] A. Moffet, "Minimum-redundancy linear arrays," *IEEE Trans. Antennas Propag.*, vol. 16, no. 2, pp. 172–175, Mar. 1968.

[16] P. P. Vaidyanathan and P. Pal, "Sparse sensing with co-prime samplers and arrays," *IEEE Trans. Signal Process.*, vol. 59, no. 2, pp. 573–586, Feb. 2011.

[17] C. Bencivenni, M. Ivashina, R. Maaskant, and J. Wettergren, "Synthesis of maximally sparse arrays using compressive sensing and full-wave analysis for global earth coverage applications," *IEEE Trans. Antennas Propag.*, vol. 64, no. 11, pp. 4872–4877, Nov. 2016.

[18] W. Roberts, L. Xu, J. Li, and P. Stoica, "Sparse antenna array design for MIMO active sensing applications," *IEEE Trans. Antennas Propag.*, vol. 59, no. 3, pp. 846–858, Mar. 2011.

[19] T.-J. Shan, M. Wax, and T. Kailath, "On spatial smoothing for direction-of-arrival estimation of coherent signals," *IEEE Trans. Acoust., Speech, and Signal Process.*, vol. 33, no. 4, pp. 806–811, Aug. 1985.

[20] C. A. Balanis, *Antenna Theory: Analysis and Design.* Wiley, 2016.

[21] P.-S. Kildal, *Foundations of Antenna Engineering: A Unified Approach for Line-of-Sight and Multipath.* Artech House, 2015.

[22] TU/e, *Phased array and smart antennas, TU/e Course.* Eindhoven University of Technology, 2020.

[23] R. J. Mailloux, *Phased array antenna handbook.* Artech house, 2017.

[24] M. N. M. Kehn, M. V. Ivashina, P.-S. Kildal, and R. Maaskant, "Definition of unifying decoupling efficiency of different array antennas–case study of dense focal plane array feed for parabolic reflector," *AEU–Int. J. Electron. Commun.*, vol. 64, no. 5, pp. 403–412, May 2010.

[25] M. V. Ivashina, M. N. M. Kehn, P.-S. Kildal, and R. Maaskant, "Decoupling efficiency of a wideband vivaldi focal plane array feeding a reflector antenna," *IEEE Trans. Antennas Propag.*, vol. 57, no. 2, pp. 373–382, Feb. 2009.

[26] K. F. Warnick, R. Maaskant, M. V. Ivashina, D. B. Davidson, and B. D. Jeffs, *Phased Arrays for Radio Astronomy, Remote Sensing, and Satellite Communications.* UK: Cambridge University Press, 2018.

[27] D. Tse and P. Viswanath, *Fundamentals of Wireless Communication.* Cambridge University Press, 2005.

[28] A. Goldsmith, *Wireless communications.* Cambridge university press, 2005.

[29] R. W. Heath and A. J. Paulraj, "Switching between diversity and multiplexing in MIMO systems," *IEEE Trans. Commun.*, vol. 53, no. 6, pp. 962–968, Jun. 2005.

[30] L. Zheng and D. N. C. Tse, "Diversity and multiplexing: A fundamental tradeoff in multiple-antenna channels," *IEEE Trans. Inf. Theory*, vol. 49, no. 5, pp. 1073–1096, May 2003.

[31] Q. H. Spencer, C. B. Peel, A. L. Swindlehurst, and M. Haardt, "An introduction to the multi-user MIMO downlink," *IEEE Commun. Mag.*, vol. 42, no. 10, pp. 60–67, Oct. 2004.

[32] M. T. Ivrlac and J. A. Nossek, "Toward a circuit theory of communication," *IEEE Trans. Circuits Syst. I, Regul. Pap.*, vol. 57, no. 7, pp. 1663–1683, Jul. 2010.

[33] N. Chiurtu, B. Rimoldi, E. Telatar, and V. Pauli, "Impact of correlation and coupling on the capacity of MIMO systems," in *Proc. 3rd IEEE Int. Sym. Signal Process. Inf. Technol.*, 2003, pp. 154–157.

References

[34] Y. Fei, Y. Fan, B. K. Lau, and J. S. Thompson, "Optimal single-port matching impedance for capacity maximization in compact MIMO arrays," *IEEE Trans. Antennas Propag.*, vol. 56, no. 11, pp. 3566–3575, Nov. 2008.

[35] G. R. Lockwood, P.-C. Li, M. O'Donnell, and F. S. Foster, "Optimizing the radiation pattern of sparse periodic linear arrays," *IEEE Trans. Ultrason., Ferroelectr., Freq. Control*, vol. 43, no. 1, pp. 7–14, Jan. 1996.

[36] R. L. Haupt, "Thinned arrays using genetic algorithms," *IEEE Trans. Antennas Propag.*, vol. 42, no. 7, pp. 993–999, Jul. 1994.

[37] C. A. Balanis, "Antenna theory: A review," *Proc. IEEE*, vol. 80, no. 1, pp. 7–23, Jan. 1992.

[38] W. L. Stutzman and G. A. Thiele, *Antenna theory and design.* John Wiley & Sons, 2013.

[39] A. R. Thompson, J. M. Moran, and G. W. Swenson, *Interferometry and synthesis in radio astronomy.* 3rd ed. Springer, 2017.

[40] D. Schaubert, T.-H. Chio, and H. Holter, "TSA element design for 500-1500 MHz array," in *Proc. IEEE AP-S Symp.*, vol. 1, 2000, pp. 178–181.

[41] B. Smolders, "Random sparse arrays: An option for SKAI?" Citeseer, Tech. Rep., 1998.

[42] W. Van Cappellen, S. Wijnholds, and J. Bregman, "Sparse antenna array configurations in large aperture synthesis radio telescopes," in *Proc. IEEE 3rd Eur. Radar Conf.*, 2006, pp. 76–79.

[43] J. Yu, V. A. Khlebnikov, and M.-H. Ka, "Wideband grating-lobe suppression by rotation of the phased array stations in the SKA low-frequency sparse aperture array," *IEEE Trans. Antennas Propag.*, vol. 63, no. 9, pp. 3939–3946, Sep. 2015.

[44] O. M. Bucci, S. Perna, and D. Pinchera, "Synthesis of isophoric sparse arrays allowing zoomable beams and arbitrary coverage in satellite communications," *IEEE Trans. Antennas Propag.*, vol. 63, no. 4, pp. 1445–1457, Apr. 2015.

[45] H. Unz, "Linear arrays with arbitrarily distributed elements," *IRE Trans. Antennas Propag.*, vol. 8, no. 2, pp. 222–223, Mar. 1960.

[46] R. Harrington, "Sidelobe reduction by nonuniform element spacing," *IRE Trans. Antennas Propag.*, vol. 9, no. 2, pp. 187–192, Mar. 1961.

[47] A. Ishimaru, "Theory of unequally-spaced arrays," *IRE Trans. Antennas Propag.*, vol. 10, no. 6, pp. 691–702, Nov. 1962.

[48] R. Willey, "Space tapaering of linear and planar arrays," *IRE Trans. Antennas Propag.*, vol. 10, no. 4, pp. 369–377, Jul. 1962.

[49] A. Maffett, "Array factors with nonuniform spacing parameter," *IRE Trans. Antennas Propag.*, vol. 10, no. 2, pp. 131–136, Mar. 1962.

[50] O. M. Bucci, T. Isernia, S. Perna, and D. Pinchera, "Isophoric sparse arrays ensuring global coverage in satellite communications," *IEEE Trans. Antennas Propag.*, vol. 62, no. 4, pp. 1607–1618, Apr. 2014.

[51] C. Bencivenni, M. Ivashina, R. Maaskant, and J. Wettergren, "Design of maximally sparse antenna arrays in the presence of mutual coupling," *IEEE Antennas Wireless Propag. Lett.*, vol. 14, pp. 159–162, 2015.

[52] J. Vespoli, F. Haber, R. Berkowitz, and D. Yavuz, "A self-organizing random array communications relay," *IEEE Trans. Commun.*, vol. 31, no. 4, pp. 484–492, Apr. 1983.

[53] D. Yavuz, "Frequency and focal region properties of random sparse arrays," *IEEE Trans. Antennas Propag.*, vol. 32, no. 5, pp. 456–465, May 1984.

[54] S. Holm, B. Elgetun, and G. Dahl, "Properties of the beampattern of weight- and layout-optimized sparse arrays," *IEEE Trans. Ultrason., Ferroelectr., Freq. Control*, vol. 44, no. 5, pp. 983–991, Sep. 1997.

[55] C. Z. Cooley, M. W. Haskell, S. F. Cauley, C. Sappo, C. D. Lapierre, C. G. Ha, J. P. Stockmann, and L. L. Wald, "Design of sparse halbach magnet arrays for portable MRI using a genetic algorithm," *IEEE Trans. Magn.*, vol. 54, no. 1, Jan. 2018, Art. no. 5100112.

[56] B. Diarra, M. Robini, P. Tortoli, C. Cachard, and H. Liebgott, "Design of optimal 2-D nongrid sparse arrays for medical ultrasound," *IEEE Trans. Biomed. Eng.*, vol. 60, no. 11, pp. 3093–3102, Nov. 2013.

[57] A. Trucco, "Thinning and weighting of large planar arrays by simulated annealing," *IEEE Trans. Ultrason., Ferroelectr., Freq. Control*, vol. 46, no. 2, pp. 347–355, Mar. 1999.

[58] N. Amani, C. Bencivenni, A. A. Glazunov, M. V. Ivashina, and R. Maaskant, "MIMO channel capacity gains in mm-wave LOS systems with irregular sparse array antennas," in *Proc. IEEE-APS Topical Conf. Antennas Propag. Wireless Commun.*, 2017, pp. 264–265.

[59] −, "Guidelines on how to plan LoS MIMO for point-to-point fixed service links," [online] Available: *https://www.ecodocdb.dk/download/279a6406-5db4/ECCRep258.pdf*, Jan. 2017.

References

[60] F. Bohagen, P. Orten, and G. Oien, "Construction and capacity analysis of high-rank line-of-sight MIMO channels," in *Proc. IEEE Wireless Commun. Netw. Conf.*, vol. 1, 2005, pp. 432–437.

[61] C. Bencivenni, M. Coldrey, R. Maaskant, and M. Ivashina, "Aperiodic switched array for line-of-sight MIMO backhauling," *IEEE Antennas Wireless Propag. Lett.*, vol. 17, no. 9, pp. 1712–1716, Sep. 2018.

[62] O. B. Sheynin, "Studies in the history of probability and statistics. XXI. On the early history of the law of large numbers," *Biometrika*, vol. 55, no. 3, pp. 459–467, Nov. 1968.

[63] F. M. Dekking, C. Kraaikamp, H. P. Lopuhaä, and L. E. Meester, *A Modern Introduction to Probability and Statistics: Understanding why and how.* Springer Science & Business Media, 2005.

[64] X. Gao, O. Edfors, F. Rusek, and F. Tufvesson, "Massive MIMO performance evaluation based on measured propagation data," *IEEE Trans. Wireless Commun.*, vol. 14, no. 7, pp. 3899–3911, Jul. 2015.

[65] Y. Aslan, A. Roederer, and A. Yarovoy, "System advantages of using large-scale aperiodic array topologies in future mm-wave 5G/6G base stations: An interdisciplinary look," *IEEE Syst. J.*, Jan. 2021.

[66] M. Grant and S. Boyd, "CVX: Matlab software for disciplined convex programming, version 2.1," 2014.

[67] D. Pinchera, M. D. Migliore, and G. Panariello, "Synthesis of large sparse arrays using IDEA (inflating-deflating exploration algorithm)," *IEEE Trans. Antennas Propag.*, vol. 66, no. 9, pp. 4658–4668, Sep. 2018.

[68] D. Pinchera, F. Schettino, M. Lucido, and M. D. Migliore, "Efficient and effective synthesis of large arrays for 5G and beyond," in *Proc. 14th IEEE Eur. Conf. Antennas Propag. (EuCAP)*, 2020, pp. 1–5.

[69] G. Oliveri, G. Gottardi, F. Robol, A. Polo, L. Poli, M. Salucci, M. Chuan, C. Massagrande, P. Vinetti, M. Mattivi, R. Lombardi, and A. Massa, "Co-design of unconventional array architectures and antenna elements for 5G base stations," *IEEE Trans. Antennas Propag.*, vol. 65, no. 12, pp. 6752–6767, Dec. 2017.

[70] G. Oliveri, G. Gottardi, and A. Massa, "A new meta-paradigm for the synthesis of antenna arrays for future wireless communications," *IEEE Trans. Antennas Propag.*, vol. 67, no. 6, pp. 3774–3788, Jun. 2019.

[71] H. Krim and M. Viberg, "Two decades of array signal processing research," *IEEE Signal Process. Mag.*, vol. 13, no. 4, pp. 67–94, Jul. 1996.

[72] H. L. Van Trees, *Optimum array processing: Part IV of detection, estimation, and modulation theory.* John Wiley & Sons, 2004.

[73] R. Schmidt, "Multiple emitter location and signal parameter estimation," *IEEE Trans. Antennas Propag.*, vol. 34, no. 3, pp. 276–280, Mar. 1986.

[74] C. A. Balanis and P. I. Ioannides, *Introduction to smart antennas.* Morgan & Claypool Publishers, 2007.

[75] TU/e, *Adaptive array signal processing, TU/e Course.* Eindhoven University of Technology, 2018.

[76] W. Melvin and J. Scheer, *Principles of modern radar: advanced techniques.* SciTech Publishing, 2013.

[77] P. Pal and P. Vaidyanathan, "Nested arrays: A novel approach to array processing with enhanced degrees of freedom," *IEEE Trans. Signal Process.*, vol. 58, no. 8, pp. 4167–4181, Aug. 2010.

[78] S. Shakeri, D. D. Ariananda, and G. Leus, "Direction of arrival estimation using sparse ruler array design," in *Proc. 13th IEEE Int. Workshop Signal Process.*, 2012, pp. 525–529.

[79] W.-K. Ma, T.-H. Hsieh, and C.-Y. Chi, "DOA estimation of quasi-stationary signals with less sensors than sources and unknown spatial noise covariance: a Khatri–Rao subspace approach," *IEEE Trans. Signal Process.*, vol. 58, no. 4, pp. 2168–2180, Apr. 2010.

[80] F. Roos, P. Hügler, L. L. T. Torres, C. Knill, J. Schlichenmaier, C. Vasanelli, N. Appenrodt, J. Dickmann, and C. Waldschmidt, "Compressed sensing based single snapshot DoA estimation for sparse MIMO radar arrays," in *Proc. 12th German Microw. Conf. (GeMiC)*, 2019, pp. 75–78.

[81] C. Waldschmidt, J. Hasch, and W. Menzel, "Automotive radar: From first efforts to future systems," *IEEE J. Microw.*, vol. 1, no. 1, pp. 135–148, 2021.

[82] F. Roos, P. Hügler, J. Bechter, M. A. Razzaq, C. Knill, N. Appenrodt, J. Dickmann, and C. Waldschmidt, "Effort considerations of compressed sensing for automotive radar," in *Proc. IEEE Radio Wireless Symp.*, 2019, pp. 1–3.

[83] H. Huawei, "Antenna structure: impact on MIMO transmission and remaining modeling issues," *3GPP TDocs Meet. id R1-86*, Aug. 2016. [Online]. Available: https://www.3gpp.org/DynaReport/TDocExMtg-R1-86-31663.htm